Published in final edited form as:

Nanoscale. 2016 May 19; 8(20): 10471–10490. doi:10.1039/c5nr08768f.

Man-Made Rotary Nanomotors: A Review of Recent Development

Kwanoh Kim[1], **Jianhe Guo**[2], **Z. X. Liang**[2], **F. Q. Zhu**[3], and **D. L. Fan**[1,2,*]

[1]Department of Mechanical Engineering, The University of Texas at Austin, Austin, TX 78712, USA

[2]Materials Science and Engineering Program, Texas Materials Institute, The University of Texas at Austin, Austin, TX 78712, USA

[3]NovaMinds, LLC, 9535 Ketona Cv. Austin, TX 78759, USA

Abstract

The development rotary nanomotors is an essential step towards intelligent nanomachines and nanorobots. In this article, we review the concept, design, working mechanisms, and applications of the state-of-the-art rotary nanomotors made from synthetic nanoentities. The rotary nanomotors are categorized according to the energy sources employed to drive the rotary motion, including biochemical, optical, magnetic, and electric fields. The unique advantages and limitations for each type of rotary nanomachines are discussed. The advances of rotary nanomotors is pivotal for realizing dream nanomachines for myriad applications including microfluidics, biodiagnosis, nano-surgery, and biosubstance delivery.

1. Introduction

Miniaturized machines and robots that can perform complicated tasks on an ultra-small scale, such as nanosurgery, have profound implications for human health.[1,2] For the last few decades, with the vigorous progress in microelectronics and nanofabrication,[3] rapid development has been made in miniaturized machines, including a variety of micro/nanoscale sensors and actuators for applications in cargo transport,[4–6] drug delivery,[7–9] biochemical sensing,[10–12] and cell trapping and biopsy.[13] Rotary nanomotors are a type of nanoscale devices that can convert different energy sources, such as acoustic,[14] electric,[15] optical,[16] magnetic,[17] and chemical[18] energies into mechanical rotations. Although their versatility and great potential have attracted intense interest, the development of miniaturized rotary motors has been greatly hindered due to significant technical challenges. For instance, micro/nanomotors made by traditional lithographical techniques suffer from complicated and arduous fabrication processes,[19,20] low yield,[21] short lifetime,[22] and low energy conversion efficiencies.[7,23]

It is highly desirable to explore new working mechanisms, designs, and approaches to resolve the encountered issues in the traditional rotary micro/nanomotors. The new concept

*Correspondence can be addressed to: ; Email: dfan@austin.utexas.edu.

of using nanoscale particles as building blocks for rotary nanomachines received considerable attention. Billions of nanoparticles can be synthesized with high efficiency and at low cost.[24,25] The tailorable dimensions of synthesized nanoentities readily allow the size of traditional NEMS motors to reduce from hundreds of micrometers to nanometers.[15,26] The tunable chemical, mechanical, and electromagnetic properties equip nanomachines with unique functions. With these great advantages, a number of device concepts, working mechanisms, and applications of rotary nanomotors made from synthesized nanoentities have been investigated.

In this article, we review the recent exciting research progresses of rotary nanomotors made of synthetic nanoparticles. The nanomotors will be categorized according to the employed energy sources including biochemical fuels, optical, magnetic, and electric fields. The advantages and drawbacks of each type of nanomotors will be discussed along with the perspectives and challenges of this rapidly developing field.

2. Biochemical Powered Nanomotors

2.1. Bio-Inorganic Hybrid Nanomotors

In biological systems, molecular machines are commonly used to perform coordinated actuations, which can efficiently convert biochemical energy existing in the surrounding medium into mechanical motions and work. Such molecules include kinesin,[27] myosin,[28] ribonucleic acid (RNA) polymerase,[29] and adenosine triphosphate (ATP) synthase.[21,30–32]

The use of the molecular machines for powering inorganic nanoentities promises the next generation NEMS/nanorobotic devices. The first demonstration was accomplished by Soong *et. al.* by using F_1-ATPase enzyme molecules as the driving component of nanomotors and lithographically patterned Ni nanorods (150 nm in diameter and 750 – 1400 nm in length) as rotors [Figure 1(A)].[21] Hydrolyzing ATP, the molecular motors successfully drove the rotational motion of the Ni propellers at a speed of 0.74 to 8.3 rps (revolutions per second). However, due to the complexity of the conjugation of inorganic nanorods to the molecular motors, only a few Ni propellers out of hundreds can be successfully assembled and rotated. In addition, limited by the nature of biomolecular motors and the low controllability of the assembling process, neither the rotation orientation nor speed can be well controlled. The lifetime of the devices was seconds to minutes.

Mano and Heller demonstrated the propulsion of carbon fibers-bioelectrocatalyst hybrid structures.[33] Glucose oxidase (GOx) and bilirubin oxidase (BOD) connected with a conductive carbon fiber (4 – 8 mm in length) was floating and moving at the interface between the glucose-containing liquid and the 1 atm O_2 atmosphere due to the oxidation of glucose at the GOx end and the reduction of O_2 at the BOD end. This redox reaction induced a pH gradient and consequent water flow, which compelled the hybrid structures to move [Figure 1(B)]. These hybrid structures not only transported but also rotated around the GOx when the ratio of GOx/BOD $\gg$1.

Micromotors based on motile microorganisms are also of great interest. With the strategically designed asymmetrical ratchet gears, Leonardo *et al.* used *E. coli* cells to power

the rotation of microgears.[34] The random motions of the *E. coli* cells in a solution are rectified on the asymmetric ratchet teeth, which exert a net torque effectively. As a result, the gears can be rotated [Figure 1(C)].

2.2. Catalytic Nanomotors

Since the first demonstration of self-propulsion of nanoentities in a hydrogen peroxide solution was reported,[35,36] catalytic nanomotors has attracted intensive attention. Catalytic nanomotors gain momentum from the decomposition of the surrounding fuel solutions. In order to acquire net force, they are designed to have asymmetric compositions and geometries such as multisegment Pt/Au nanorods[4,35,37] and Pt/SiO_2 Janus particles.[38,39] Hydrogen peroxide has been most widely used as a fuel solution. It decomposes into water and oxygen ($2H_2O_2$ (l)$\rightarrow$ $2H_2O$ (l)+ O_2(g)) on surfaces of the Pt catalysts, which results in the conversion of chemical energy into mechanical motion. Recently, water,[40,41] acid,[42] hydrazine,[43] bromine and iodine[44] solutions were explored as alternative fuels for improved performance or high biocompatibility. Although it is obvious that the decomposition of the fuel solutions results in mechanical propulsion, significant efforts are required to understand the mechanisms. Two different mechanisms have been proposed: self-electrophoresis and bubble propulsion.[45] It is found that catalytic motors comprised of a catalytic and a non-catalytic metal (*e.g.*, Pt/Au) transport with the catalyst segment as the front end. Investigations attribute the propulsion to the electric field generated from the distinct chemical potentials of the two materials, which is self-electrophoresis. On the other hand, it is found that nanomotors composed of a catalyst and an insulator (e.g., Pt/SiO_2) transport towards the end of the insulator. The propulsion force is attributed to the generation of bubbles on the surface of the catalyst segment. Most catalytic motors transport linearly in a fuel solution for cargos delivery. Recently, with in-depth understanding and sophisticated designs, some catalytic motors can be compelled to rotate. In the following, we will discuss the structure, fabrication, and motion characteristics of rotary catalytic nanomotors.

Catchmark *et al.* demonstrated the rotation of Au microgears with Pt coated on the teeth in fuel solutions [Figure 2(A)].[46] The rotation orientation was determined by the location of Pt as the Pt-coated side of the teeth moved forward due to self-electrophoresis. The diameter of the microgears was 150 μm and they were rotating in a mixture of peroxymonosulfuric acid/ hydrogen peroxide/ sulfuric acid/DI water (approximately 0.1:1:2:100) at a speed of 1 rps.

The rotation of the electrodeposited Au/Ni nanorod (2 and 0.5 μm in length, respectively) was observed in a hydrogen peroxide solution.[36] The nanorods showed two different behaviors: rotation and revolution. The rotational motion resembles the movement of clock arms. While their Au ends attached to the substrate due to either impurities or defects on the substrate, the other Ni ends rotated freely [Figure 2(B)]. The nanowire also revolved around certain circular trajectories possibly due to their asymmetric shapes that prevented them from moving along a straight trajectory. Qin *et al.* patterned Cr/Au thin films on Au-Pt-Au nanorods to expose only small areas of Pt on one side of the nanorods. Specifically, Au-Pt-Au nanorods were dispersed on a substrate and Cr/Au thin films were deposited via evaporation on their surfaces [Figure 2(C)].[18] On such structures, bubbles only generate on the areas of the exposed Pt and propel the nanorods with net torque. The rotation speed and

torque were controlled by the composition of Au/Pt as well as the location of the Pt segments in each nanorod. In another experiment, Wang *et al.* fabricated asymmetric nanorods with additional layers of Pt-Au-Cr/SiO_2/Cr deposited on one side of Au/Ru nanorods [Figure 2(D)].[47] The metal coating enables an extra force in the transverse direction along with the propulsion force in the long direction of the nanowires. In a 15% H_2O_2 solution, they rotate at an average speed of 180 rpm. One of the nanomotors reached a speed as high as ~400 rpm.

Vicario *et al.* demonstrated rotation of tethered microspheres coated with catalysts [Figure 2(E)].[48] The catalysis of hydrogen peroxide generated bubbles, which thrust the micromotors into rotation due to the composition asymmetry.

Rotary catalytic nanomotors with more complex 3D structures were obtained via dynamic shadow growth (DSG). He *et al.* fabricated linear and L-shaped Si nanorods with catalytic Pt or Ag coated on the tips [Figure 2(F)].[49] The catalysts were deposited with controlled incident angles so that they were asymmetrically located on one side of the nanorods. With the DSG technique, even Si/Ag nanosprings can be created. They rolled like screw propellers in a fuel solution.

Using the DSG technique, Gibbs and Zhao grew Pt/TiO_2 arms on silica microspheres, which worked as catalytic rotors [Figure 2(G)].[50] The rotation speed increased with the hydrogen peroxide concentration and decreased with the addition of sodium dodeclysulphate (SDS) that changed surface tension. In the following study, interlocked tadpole-like nanomotors [Figure 2(H), i] or helicopter nanomotors with V-shaped Pt/TiO_2/Ni nanorods and Ni-coated SiO_2 microbeads [Figure 2(H), ii] were assembled based on either van der Waals or magnetic interaction and demonstrated different rotation behaviors from those made of single structures with modified trajectories and postures.[51]

More recently, Gibbs and Fischer fabricated catalytic microdrills.[52] A turn of SiO_2 helix (400 ± 200 nm in diameter) was deposited on a 1-μm-diameter SiO_2 microbead through glancing angle deposition (GLAD) and the helix was asymmetrically coated with Pt. This process was repeated several times to produce helical catalytic microdrills (4 ± 1 μm in length) [Figure 2(I)]. In a H_2O_2 solution, the catalytic helices showed various types of motion, including transport, rotation around the helical axis, and combined translation and rotatory motions. Among 134 helices, a significant percentage (~25%) rotated around their moving direction like microdrills. The drilling motion can be attributed to two factors: the torque due to the asymmetrically deposited Pt layers on the helices and the interaction between the rotation and the linear propulsion of the helical structures in the low Reynolds number regime of the suspension.

Solovev *et al.* reported another type of catalytic nanodrill based on the bubble propulsion mechanism.[53] Rolled-up InGaAs/GaAs/Cr/Pt nanotubes with Pt at the inner walls of the tubes produced bubbles in a H_2O_2 solution. The nanotubes obtained momentum by releasing bubbles from their inside, or self-propulsion. Moreover, torques can be generated on asymmetrically rolled-up nanotubes, which compel the nanotubes along a spiral trajectory like a drill [Figure 2(J)]. Here, an iron thin film deposited on the nanotubes assists direction

control with magnetic fields. These nanodrills were transported, drilled, and stuck into HeLa cells successfully.

As aforediscussed, hydrogen peroxide is one of the most widely used fuel solutions for catalytic nanomotors. However, the potential applications are greatly compromised by its corrosive nature to biological substances. To resolve this issue, it is essential to explore alternative biocompatible fuels to power the catalytic motors. Liu *et al.* reported collective motions of $(Pb_{0.25}Ba_{0.15}Sr_{0.6})TiO_3$ (PBST) nanotubes in DI water [Figure 2(K)].[54] The nanotubes were synthesized by electrodeposition into nanoporous templates and one end of the nanotube arrays was sealed with nail oils. The alumina templates were dissolved in potassium hydroxide (KOH) solutions, where KOH filled into the nanotubes through the open ends. When the nanotube arrays were placed in DI water, the K^+ ions were released from one-end of the nanotubes, which effectively propelled the nanotubes to rotate owing to chemical gradient of K^+ ions. The rotation continued for ~15 s and stopped due to the reduction of concentration gradient of the K^+ ions. The speed was as high as 30 rps.

Liu *et al.* introduced Cu-based nanomotors working in Br_2 and I_2 solutions.[44] This type of nanomotors consumes Cu in the reaction that propels the motion. First, Cu nanowires were deposited into nanoporous templates. Instead of chemically etching the seed layer sputtered at the bottom of the templates, the authors mechanically polished it and deformed one end of the nanowires [Figure 2(L)]. Due to the asymmetric structure, the chemical reaction rate on each end of the nanowires became different, which resulted in ionic gradient that induced torques and rotated the nanotubes in Br_2 or I_2 solutions. In comparison, symmetric nanowires of the same composition have no observable continuous rotary motions.

Harnessing chemical energy in surrounding medium, rotary catalytic nanomotors are unique and attractive in that their autonomous motions, requiring no external power sources.[23] However, most rotations powered by catalytic reactions still have a relatively large degree of randomness, *i.e.*, a large portion of nanomotors do not rotate or move in a defined fashion. A high precision control in the composition and structures of the nanomotors is necessary to mitigate this problem. It is also essential to control the rotation orientation and to tune the speed precisely. More investigations on new biocompatible fuels or powering catalytic mechanisms are critical for biomedical applications.

3. Physical-Field-Driven Rotary Nanomotors

Recently, significant advances have been achieved in physical-field-driven rotary nanomotors. Compared to biological hybrid nanomotors or catalytic nanomotors, they are advantageous in the high controllability in rotation angle, speed, and orientation. Some types of rotary nanomotors can operate in ordered arrays at designated positions. The speed is as high as 18,000 rpm.[15] The lifetime can reach 80 hours with over 1.1 million cycles.[55] Physical-field-driven rotary nanomotors are also advantageous in the overall biocompatibility and facileness in device integration. In the following discussion, we will categorize rotary nanomotors according to the employed external fields including the magnetic, optical, and electric fields.

3.1. Magnetic Tweezers

Magnetic field driven micro/nanomanipulation have been widely used in biomedical research since Crick and Hughes employed magnetic particles to study physical properties of cytoplasm in 1950.[56] Magnetic fields are usually created in two manners. With permanent magnets, one can facilely generate strong external magnetic fields. However, it is difficult to adjust the field intensity or change the orientation. Because of this, solenoid electromagnets are more widely used in recent studies. Orthogonal sets of Helmholtz coils are arranged in X, Y, and Z directions, which can produce uniform and tunable magnetic fields independently in each dimension. By applying sinusoidal currents with sequential phase shifts to each Helmholtz coil set, a rotating magnetic field can be readily created to rotate nanoentities.

With magnetic fields, nanoparticles with embedded magnetic materials can be driven to align, chain, transport and rotate in a non-contact fashion. The actuation is effective in essentially any suspension mediums, such as water, blood, and saline solutions. It does not require additional chemicals as fuels. Even more, strong magnetic fields, such as several Tesla, can be readily applied on live beings with little side effects. Owing to the aforementioned merits, magnetic field directed manipulation has found wide applications in cutting-edge biomedical research, *e.g.*, microfluidic mixing,[57,58] winding DNA/RNA strands and probing their torsional stiffness.[59–65]

By strategically applying external magnetic fields, magnetically functionalized micro/nanoparticles and bioentities can be readily transported and rotated. The nanoparticles are aligned in the same direction of the magnetic field, while transported along the field gradients. Due to difficulties in generating strong magnetic field gradients over a large distance, the applied magnetic fields are often used for aligning and trapping rather than moving nanoparticles.[66,67] When rotating the magnetic field (B), owing to the dipole interactions, it can efficiently exert alignment torques (τ_{mag}) to rotate nanoparticles, given by $\tau_{mag} = m \times B$, where m is the magnetic moment of the nanoparticle. Here, most of the magnetic nanoentities studied in this topic are ferromagnetic with integrated components such as Ni and Co, or superparamagnetic, such as Fe_2O_3 and Fe_3O_4.

3.1.1. Magnetically Driven Screw Propellers—Although there is no net force to transport particles in a uniform magnetic field, researchers have explored new mechanisms to convert magnetic rotation into linear propulsion. Miniaturized screw propellers are one of those examples. Ishiyama and colleagues fabricated a millimeter scale cylindrical NdFeB magnets with a screw-shaped brass tip [Figure 3(A)].[68] The devices were magnetized in the transverse direction and thus rotated along the long axis in a rotating magnetic field. Although rotated in highly viscous mediums, *e.g.*, silicone oil or agar, they can move forward or backward up to more than 14 mm/s, proportional to the rotation frequency of the magnetic field until reaching a so-called threshold step-out frequency. Above the step-out frequency, the rotation speed decreases. Remarkably, linear propulsion of the magnetic nanomotors can be executed even inside a bovine tissue at a speed of ~1 mm/s in a 150 Oe/10 kHz magnetic field. In the following study, the group demonstrated the individual control of speeds of multiple devices of distinct dimensions by exploiting their different

step-out frequencies.[69] Furthermore, the nanomotors could be heated or mechanically deformed with additional AC or DC magnetic fields.

Mimicking the motions of natural flagella, Nelson's group reported artificial bacteria flagella (ABF) consisting a magnetic head (Cr/Ni/Au) and a spiral tail (either InGaAs/GaAs or InGaAs/GaAs/Cr ribbons) [Figure 3(B)].[70] The ABF can move forward and backward along the long axis depending on its rotating orientation in a 2.0 mT magnetic field. The diagonal of the square magnetic head aligned along the magnetic field, which guided the moving direction of the device. The velocity increased with the rotation speed. The ABF pushed a 6-μm-diameter PS microsphere to a speed of 3 μm/s in DI water. In depth study showed that the ABFs rotated synchronously with the applied magnetic field until reaching the step-out frequency.[71] The rotation speed and translational velocity increased with the intensity of the magnetic field (up to 18 μm/s with 2.0 mT) as well as the size of the magnetic head. While rotated, the ABFs unwantedly rolled over the substrate due to uneven viscous drag near the solid substrate. They also slightly drifted perpendicular to the moving direction. However, the overall moving direction and velocity can be well controlled in a large 3-D space by the three orthogonal sets of electromagnetic coils. Multiple ABFs can transport synchronously like a swarm. The ABFs not only directly push micro/nanoparticles but also generate liquid flows which could find useful applications in fluid pumping, mixing, and particle sorting.[72]

More recently, the same research group introduced magnetic spiral micromachines with SU-8 or IP-L polymer coils coated with Ni/Ti thin films.[73] The polymer coils were fabricated by 3-D direct laser writing (DLW)[74] with various sizes and geometries (4 – 64 μm in length, 1 – 8 μm in diameter, and 35 – 75° helix angles). At frequencies below 15 Hz, the helices just wobbled with their rotation axis misaligned with the helical axis. However, at frequencies above 15 – 40 Hz, depending on the geometry of the helices and the magnetic field strength, they overcame the wobbling and thrusted along the helical axis [Figure 3(C)]. These micromachines can work in biological mediums, such as fetal bovine serum (FBS). With integrated microholders at the tips, the helices can efficiently pick up and convey PS particles to locations at different heights. On the other hand, due to magnetic interactions, the micromachines swimming close by can assemble with each other in various forms (side-by-side, cross, and long-chain) and their moving speed and direction changed upon the assembly.[75] This is an often-observed phenomenon in magnetically manipulated particles.

In parallel, Ghosh *et al.* reported smaller screw propellers comprised of silica spherical heads (200 – 300 nm in diameter) and twisted tails (2 – 3 μm long) [Figure 3(D)].[17] Such helical nanoswimmers were fabricated via GLAD[76] of SiO_2 followed by thermal evaporation of a ferromagnetic Co thin film. The helices were magnetized along the radial direction so that they can be rotated along the long axis in a rotating magnetic field and produced thrusts. A magnetic field of 50 – 60 G was applied at frequencies up to 170 Hz. The helices reached a translational speed of ~40 μm/s. They could be guided through programmed paths, *i.e.*, spelling alphabets, which demonstrated the high controllability of the manipulation. These helical nanoswimmers showed different rotation modes depending on the frequency of the magnetic field.[77] They rotated around the short axis at a low frequency, while gradually switched to long-axis rotation with increased frequencies before

it reached the step-out frequencies. Such helical nanomachines can readily work in complex non-Newtonian biological medium such as blood,[78] glycerol-water mixture, and Hyaluronan solutions.[79] Their sizes can be further reduced to submicrometers. Although these tiny nanomachines were under severe perturbation and can hardly transport in DI water due to Brownian motions, they worked reliably in highly viscous mediums. Furthermore, it is found from experiments and numerical computations that the optimal length of the nanoswimmers is only slightly longer than one helical turn, much shorter than most of the reported nanoswimmers.[80] This is due to the balance between the net chirality of the propulsion and the viscous drag, both increase with the length of the helices. Based on this finding, the nanoswimmers can be further miniaturized without performance compromised. The fabrication time and cost can also be reduced.

Although various techniques, including 3D DLW and GLAD, have been developed, the fabrication of 3D helical micro/nanostructures is still a daunting task. Different research groups are exploring high throughput and low cost fabrication methods. Inspired by the electrodeposition of Pd nanosrping,[81] Li *et al.* fabricated helical magnetic nanoswimmers [Figure 3(E)].[82] Pd/Cu alloys electrodeposited in nanoporous templates formed into spiral crystal nanostructures. The templates and Cu were sequentially dissolved and Ni was evaporated. As a result, Ni-coated Pd nanosprings can be obtained. The diameter and pitch length were precisely controlled by the pore size of the templates and the composition of the Pd^{2+}/Cu^{2+} in the electrolytes. The Ni-coated Pd nanosprings worked as screw propellers in a rotating magnetic field with a speed of ~15 μm/s in a 150 Hz magnetic field.

In another approach, Gao *et al.* innovatively made helical magnetic micropropellers by using vascular plants as templates.[83] They extracted coiled vessels from leaves of plants, modified the diameters and pitches by stretching the coils, and deposited thin films of magnetic Ti/Ni [Figure 3(F)]. Finally, the magnetically functionalized coiled vessels were trimmed into small pieces of 30 – 60 μm in length. These coils can be compelled as micro-swimmers in 10 G rotating magnetic fields at 10 – 80 Hz with a maximum speed of 250 μm/s (~5 body length/s).

3.1.2. Magnetic Nanoswimmers with Flexible Joints—Distinct from the aforediscussed magnetic helical propellers, Wang *et. al.* reported another type of flagella-like nanoswimmers manipulated by rotating magnetic fields.[84] This type of nanomachines consisted of rigid Ni and Au segments connected by a flexible Ag segment. Owing to the flexible Ag joint, the Ni and Au segments at each end both rotated, however, at different amplitudes. This asymmetric behavior resulted in unidirectional propulsion. Depending on the length of the Ni and Au segments, the devices moved forward (with the Ni segment pushing the device) or backward [Figure 3(G)]. Their motions including the translational velocity can be controlled by the frequency of the rotating magnetic field in the range of 0 – 15 Hz. The devices have successfully worked in biological mediums, such as urine. Following this study, the group demonstrated targeted drug delivery with the flexible Ni/Ag nanoswimmers.[9] The nanoswimmers picked up and transported drug-loaded magnetic microparticles to cancer cells in a microfluidic channel filled with a cell culture medium. Although large cargoes over 2 μm in diameter could change the rotational and translational

motion of the nanoswimmers substantially, the microparticles used for drug delivery (1.25 μm in diameter) did not slow the nanoswimmers significantly.

3.1.3. Nanomachines Walking along Solid Boundaries—Rotating magnetic nanomachines can also tumble and walk near liquid-solid boundaries. When placed near solid boundaries, *e.g.*, walls or substrates, rotating elongated micro/nanoparticles can transport in plane. It is due to the asymmetric viscous drag received on each end of the nanostructures, where the drag force is higher near the solid surface than that in the bulk solution. Due to this asymmetry, the tangential speed of the rotating object near the solid boundary is slower than the other end, which results in the transport of objects near the boundaries like wheels rolling on the road.

Tierno *et al.* demonstrated translation of paramagnetic doublets linked with DNA pairs owing to magnetic rotations near the glass substrates [Figure 4(A)].[85] Their precession angle was adjusted with an additional static magnetic field $\mathbf{H_0}$ along with the rotating field $\mathbf{H_1}$ and the H_0/H_1ratio. It is found that the frequency of H_1 determined the translational velocity. Assemblies of paramagnetic particles with various sizes, numbers of particles, and link shapes were readily transported and guided through grooves patterned on the glass substrate.[86] Furthermore, the behaviors of the colloidal particles were studied analytically. More efficient propulsions can be achieved from elliptic magnetic fields than that from circular magnetic fields.[87]

Sing *et al.* reported self-assembled superparamagnetic particles working as micro-rotors.[88] The particles formed into chains, which rotated as single objects in a rotating magnetic field. They transported due to interactions with solid boundaries, *i.e.*, the substrates [Figure 4(B)]. The translational velocity increased with the frequency of the rotating magnetic field and the number of particles in a chain at a low frequency. However, the particle chains broke into multiple segments at high frequencies, which slowed the translational motion significantly. The rotation of the particle chains also created liquid flows in the surroundings, which can convey a large vesicle in a microfluidic device.

Zhang *et al.* directly employed Ni nanowires as rotors.[89] They prepared the nanowires by electrodeposition into nanoporous templates. The nanowires were rotated laterally near the vertical wall in a rotating magnetic field and moved along the wall due to the asymmetric boundary conditions at each end [Figure 4(C)]. The maximum translational velocity of ~37 μm/s was achieved from a 12-μm-long nanowire in a magnetic field of 2 mT at 35 Hz. The nanowire rotors can also transport near substrates without a vertical wall to pick up, transport, and release 6-μm-diameter PS spheres. This magnetic manipulation mechanism was also applicable to biological systems. For instance, rotating Ni nanowires were employed to drive synthetic polymer particles, microorganisms and human blood cells to desired locations, which could be useful in bio-particle assembling and targeted delivery.[90]

3.1.4. Microdrills with Rolled-Up Microtubes—Wang *et al.* demonstrated magnetically driven microdrills using rolled-up microtubes with sharp tips.[91] The trapezia patterns of Ti/Cr/Fe thin film stacks were rolled up into tubes. The diameters of the tubes (5 – 10 μm) were controlled with surface stress determined by the thickness of the thin films.

The trapezoidal pattern and asymmetric roll-up resulted in the sharp tips [Figure 4(D), i]. The tubes were rotated in a 20 mT magnetic field. They switched their rotation direction depending on the frequency of the rotating magnetic field, either horizontally (at low frequency) or vertically (at high frequency) for navigation or drilling of holes, respectively [Figure 4(D), ii]. These microdrills can be applied to make holes in a pig liver *ex vivo*. Although the microtubes cannot move on compliant or rough samples and their rotation speed decreased significantly after a few minutes of drilling, they can successfully drill holes as deep as 25 μm as shown by SEM characterizations.

3.1.5. Micofluidic Pump with Magnetic Microbeads—Köhler and his colleagues developed microfluidic pumping device comprised of a magnetically actuated microrotor [Figure 4(E)].[58] Three polystyrene microspheres were assembled as a rotor via manipulation with optical tweezers and strategical conjugation with Streptavidin-Biotin reactions. The polystyrene sphere in the center was functionalized with Streptavidin and the other two spheres were coated with magnetite and Biotin. The rotor was integrated in a microfluidic channel and driven by a rotating magnetic field. Due to the asymmetrical geometry around the rotor, the fluidic flow field around the rotor was not uniform, which generated net flows depending on the rotating direction of the rotor. At its maximum speed 120 rpm, the microrotor was able to pump the flow at a speed of 0.4 – 0.5 μm/s on average.

3.2. Optical/Plasmonic Nanomotors

Micro/nanoentities can be also rotated by optically induced torques. These optical/plasmonic nanotweezers are not only versatile in micro/nanomanipulation, including trapping, transport, and rotation, but also compatible with biological systems at suitable optical wavelengths.

3.2.1. Manipulation by Light Rotation—The optical tweezers have been widely used to trap and transport micro/nanoparticles since Arthur Ashkin observed trapped microscopic particles by a focused laser beam in 1986.[92] In 1991, Sato *et al.* demonstrated rotation of red blood cells by a high-order mode laser beam with a rotating non-uniform intensity profile, which was one of the first rotary manipulations by optical fields.[93] In the experiments, cells were aligned along the long axis of an elliptical laser beam and rotated synchronously with the beam around the optical axis. The speed was ~ 6 rpm. In the following studies, rotatable lenses and apertures were used, which provided controls over both the rotation speed and orientation.[94–96] Based on a similar strategy, Inoue *et al.* proposed a viscous micropump, which consisted of a U-shaped microchannel and a microrotor rotated by a circularly scanning three-point optical trap.[97] The average flow velocity was around 1 μm/s in this microfluidic device when the speed of the microrotor reached 30 rpm.

3.2.2. Micro/Nanomotors Driven by Angular Momentum of Light—Light carries momentums, which has both linear and angular contributions. The angular momentum has a spin component related to polarization and an orbital component related to spatial distribution. Beth made the first observation of the spin angular momentum of circularly polarized light passing through a rotating birefringent plate.[98] The change of the polarization of light when passing through a birefringent particle resulted in a rotary torque back to the

particle itself. Leveraging this mechanism, Friese *et al.* rotated calcite samples at a speed of a few thousand rpm.[99] However, this mechanism is only applicable to birefringent materials. A way to rotate non-birefringent particles is to place a spinning birefringent particle next to an optically trapped non-birefringent particle, such as a SiO_2 microgear, to compel the rotation with over 50% torque transfer efficiency [Figure 5(A)].[100]

Another optical manipulation scheme is based on the use of orbital angular momentums of light with a helical wavefront that propagates with its Poynting vector forming a corkscrew-like path [Figure 5(B)].[101–105] When such an optical beam illuminates microparticles, the orbital angular momentum of photons can be transferred, which results in net torques and rotation of the microparticles. This rotation strategy is not limited to transparent micro/nanoparticles, owing to the lately developed dark focus technique, which creates localized intensity null at the focus of optical beam. One can trap and rotate micro/nanoparticles with strong reflection and absorption of light. Note that such particles can be repelled away or damaged if manipulated by conventional optical fields with high light intensity at the focus.[106,107]

Moreover, micro/nanomotors can be manipulated by both the spin and orbital angular momentums [Figure 5(C)].[108] They are promising for pumping or mixing in microfluidics [Figure 5(D)].[107,109–112] For instance, by projecting arrays of optical vortices,[110,112] cooperative flows can be reconfigured dynamically on length scales as small as tens of nanometers.

3.2.3. Radiation Pressure Micromotors Driven by the Linear Momentum of Light—Besides angular momentum, linear momentum can rotate micro/nanoentities. As shown in Figure 5(E), an optical torque is produced in asymmetric micro-objects by a net radiation pressure.[113,114] The forces of radiation pressure are generated due to the change of the linear momentum of photons in refracted/reflected optical beams. The first radiation pressure driven rotatory micromotor was designed by Higurashi in 1994.[113] The rotation speed was precisely controlled, proportional to the incident laser power. However, the micromotors only rotated in one direction, determined by the geometry of the motors. Later, more sophisticated microstructures were designed for improved performances.[114–117] For instance, with an additional central linear axis to the rotors in the design, the micromotors can rotate more stably at a fixed position in the optical trap.[115] They also developed a micromotor with dual rotation orientations by shifting its central position upward or downward off the focal position of the incident laser beam.[116] Given the aforementioned advantages including the remote controllability, stable trapping during rotation, and precise regulation of ultra-low flow rates, various radiation pressure micromotors have been applied in microfluidics systems to generate and control microflows.[117,118] For instance, the twin spiral microrotor that rotated up to 560 rpm at a laser power of 500 mW was incorporated as a micropump in the microfluidic channel [Figure 5(F)]. This tandem micropump assembled with a pair of optical nanomotors induced directional flow along the microchannel and demonstrated long-distance transport of micropaticles.

3.2.4. Plasmonic Nanomotors—The dimensions of motors driven by conventional optical tweezers are usually micrometers to millimeters. It is arduous to further decrease the

dimensions of motors due to the weakened light–matter interactions with size reduction. To effectively enhance the light–matter interactions, plasmonic optical tweezers were developed based on plasmonic resonances in metallic nanostructures. [119–121] Since then, much smaller and efficient metallic nanomotors have been achieved. In 2009, Jones *et al.* demonstrated that Au nanorod aggregates (10 nm × 45 nm) can be rotated by anisotropic light scattering generated from the asymmetric structures. The nanorod aggregates exhibited strong plasmonic resonances in the near infrared regime with high saturation intensities, which facilitate efficient and feasible rotation [Figure 6(A)].[122] Similarly, dielectric nanospheres with strategically deposited Au patterns on the surface were compelled to rotate, owing to the asymmetrical optical scattering.[123]

In 2010, an even smaller plasmonic nanomotor was demonstrated.[16] With its strong interaction with light, the motor, only 30 nm thick and 200 nm in diameter, generated a torque sufficient to rotate a micron-size silica disk [Figure 6(B)]. This plasmonic nanomotor had an asymmetric gammadion gold structure, which induced different phase retardations in the reemitted light at different parts of the nanomotor and effectively generated torque to rotate the entire microstructure. The rotation speed and orientation were facilely tuned by the laser power and wavelength. The plasmonic effect can greatly enhance mechanical torques, which is an important advance in optically enabled nanomotor systems. Note that more works on the rotation of metallic nanowire/nanorod were demonstrated recently, based on the transfer of orbital angular momentum of light [Figure 6(C)].[121,124–126]

Overall, the plasmonic optical tweezers enable the development of much smaller and more efficient nanomotors driven by light compared to the previous works. However, the forces involve in opto-plasmonic manipulation are complex, including gradient-intensity trapping forces, radiation pressure forces, induced-electric-dipole interactions, and plasmonically-induced Lorentz forces, all of which can have significant impact on the manipulation.[127] Numerical simulations are necessary to analyze or predict how these forces attribute to the fundamental manipulation mechanisms.[16,123,126]

3.3. Electrically Driven Micro/Nanomotors

Nanoentities suspended in a liquid medium can be manipulated precisely and efficiently by external electric fields. Recently, assisted with electric fields, significant progresses have been made in rotary nanomotors. In this section, we will discuss various types of electric micro/nanomotors including the design, working mechanisms, fabrication procedures, performances, and applications.[128–130]

3.3.1. Arrays of Rotary Nanomotors Operating at Designated Positions by AC Electric Fields

3.3.1.1. Design: Most aforediscussed nanomotors rotate freely in suspension. However, for practical applications, it is arduous to use freely rotating nanoparticles to deliver torques or forces effectively. Random liquid agitations can easily disturb the mechanical motions and move away nanomotors from desired positions. In order to produce and convey controlled mechanical forces and torques, it is critical to assemble micro/nanomotors at designated locations and couple them with other micro/nano objects for functional work. Most

previously reported micro/nanomotors that rotated at fixed positions were made by top-down lithographic processes.[16,21,26] Recently, a new type of rotary nanomotors, bottom-up assembled from nanoscale building blocks, was reported.

The nanomotors rotated stably with controlled angle, speed, and orientation at fixed locations and their speed reached at least 18,000 rpm. They were demonstrated for tunable biochemical release by controlled mechanical rotation, which was the first of its kind.[15,131] The design of such nanomotors consisted of three components: a multi-segment nanowire, patterned magnet, and quadrupole microelectrodes working as a rotor blade, bearing, and stators, respectively [Figure 7(A)]. The nanowire rotor was magnetically anchored on a patterned nanodisk due to magnetic attractions and compelled to rotate by external electric fields. The nanowire and nanodisk were carefully designed so that the magnetic attraction force was strong enough to anchor the nanowire on the nanodisk bearings while still allowing the rotation. Multi-segment nanowires with embedded magnetic segments, *e.g.*, Au/Ni/Au nanowires, were prepared by template-assisted electrodeposition in a three-electrode cell setup.[132,133] The dimensions defined by the pore size of the templates were 150 – 400 nm in diameter and 800 nm – 10 μm in the total length. Either single or multiple Ni segments were fabricated in a single nanowire with lengths of 100 nm – 1 μm. The nanodisks, with uniform diameters ranging from 200 nm – 2 μm, served as bearings. They consist of a thin film stack made of Au (or Ti)/Ni/Cr, where the magnetic Ni layer provides magnetic attraction forces to anchor the nanowire rotors onto the nanodisks, and the Au (or Ti) layer tunes the magnetic forces precisely by adjusting the distance between the magnetic layers in both the nanowires and the nanodisks.

3.3.1.2. Electric Tweezers Based on Combined AC and DC Fields for Transport and Assembling: The nanomotors were assembled by the electric tweezers, a powerful nanomanipulation technique based on the combined uniform AC and DC electric fields, which can transport nanoentities in suspension with a precision of 150 nm (or 300 nm depending on the estimation method) at a speed of at least ~80 μm/s.[129,131,134] The uniform DC and AC electric fields transport and align nanoparticles by the electrophoretic (EP) and dielectrophoretic (DEP) forces, respectively. The velocity of a nanoparticle is proportional to the DC electric field, given by:

$$v = -\frac{\varepsilon_r \varepsilon_0 \zeta}{\eta} E_{DC} \quad (1)$$

where ε_r, ε_0, ζ, and η are the permittivity of the liquid medium and free space, zeta potential, and viscosity of the medium, respectively.[134,135] Although there is no field gradient ($\nabla E = 0$) and consequently no net DEP force ($F_{DEP} \propto \nabla E^2$) in a uniform AC electric field, the particle still receives an electric torque and gets aligned in the direction of the AC field. By applying combined AC and DC electric fields in both the X and Y directions on two sets of perpendicularly configured electrode pairs, nanoentities can be transported along arbitrary trajectories and positioned at any locations at a speed as fast as 80 μm/s.[131] Not only metallic nanowires can be manipulated, essentially any materials, including metallic, semiconducting, or insulators can be manipulated by the electric tweezers. With this technique, various arrays of nanomotors can be assembled by manipulating and positioning

the nanowire rotors on the magnetic bearings one by one. Due to the high manipulation efficient, it just took ~ 10 sec to assemble one device.

3.3.1.3. Actuation of the Rotary Nanomotors: As discussed above, an AC electric field can align a prolate micro/nano-object. If placed in a rotating electric field, can the micro/nano-objects be rotated? The rotating electric field can be created by applying four AC voltages with sequential 90° phase shift to quadruple microelectrodes. Micro-objects, such as cells have been rotated with such rotating AC fields. The driving electric torque (τ_e) is proportional to the square of the applied electric field (E^2), *i.e.*, $\tau_e \propto E^2$.[135] The first continuous rotation of metallic nanowires and carbon nanotubes in a rotating electric field were achieved by Fan *et al.*[128] The work demonstrated desirable characteristics of longitudinal nano-objects as rotary nanomotors. The rotation of nanowires/nanotubes promptly started and stopped without noticeable acceleration and deceleration. The rotation speed, advantageously proportional to the square of the applied electric field (E^2), were readily tuned by the AC voltage and frequency [Figure 7(A)].[128] Not only metallic nanowires or carbon nanotubes but also semiconductor and even insulating nanowires, such as Si, ZnO and SiO_2, have been rotated.[136] The rotation characteristics are determined by electric conductivity and permeability of the manipulated nanoparticle and suspension medium, dimension of the nanoparticle, and AC frequency. Based on simple models, the electric conductivity of nanoparticles can be estimated from their mechanical rotation.[137] By pinning the center point of a bended metallic nanowire on a substrate, a nanomotor with two blades was assembled, which can drive a dust particle into continuous rotation.[128,129]

3.3.1.4. Analytic Modeling and Performance Characterization of Nanomotors in Speed, Size, and Lifetime: Now, by using the same actuation approach based on AC electric field, nanomotors consisting of nanowire rotors and magnetic bearing have been successfully rotated both clockwise and counterclockwise.

There are five torques that govern the rotation dynamics of nanomotors, given by[15]

$$\tau_e+\tau_{e'}+\tau_\eta+\tau_m+\tau_f=0 \quad (2)$$

where τ_e and $\tau_{e'}$ are the electric torques due to the external AC field and due to the interaction of the polarized nanowire and nanobearing in the AC field, respectively, τ_η, τ_m, and τ_f are the viscous torque in a liquid medium, magnetic torque between the magnetic segment of the nanowire and the Ni layer in the nanodisk, and friction torque between the nanowire and the nanodisk. Since τ_e and $\tau_{e'}$ are proportional to square of the applied voltage V^2 and τ_η linearly increases with the rotation speed (ω):

$$\omega=\left(\frac{a+b}{-c}\right)V^2+\left(\frac{\tau_m+\tau_f}{-c}\right), \quad (3)$$

where *a*, *b*, and *c* are the coefficient of τ_e, $\tau_{e'}$, and τ_η. These coefficients depend on the geometry, dimension, and electric properties of the nanowire and the suspension medium. While it is obvious that the rotation speed is a quadratic function of the applied voltage, how the magnetic interaction between nanoentities affects the rotation is complicated and depends on the magnetic interaction between the components. With a simple magnetic

dipole-dipole interaction modeling, magnetic torque τ_m and force F_m generated by the magnetic interaction between $\mathbf{m_1}$ and $\mathbf{m_2}$ in Figure 7(A) can be calculated as $\tau_m = (\mu_0 m_1 m_2/4\pi x^3) \sin\Theta$ and $F_m = (3\mu_0 m_1 m_2/4\pi x^4) \cos\Theta + c$, respectively, where μ_0 is the magnetic permittivity of vacuum and x and Θ are the distance and angle between $\mathbf{m_1}$ and $\mathbf{m_2}$. The frictional torque (τ_f) is proportional to the magnetic force (F_m) perpendicular to the interface. Therefore, the rotation speed can be further calculated as:

$$\omega = \left(\frac{a+b}{-c}\right) V^2 + \left(\frac{d\sin\Theta + e\cos\Theta}{-c}\right) \quad (4)$$

with the coefficient d and e for τ_m and τ_f respectively. This analysis agrees with experiments excellently that the magnetically induced torques results in sinusoidal fluctuating speed of nanomotors every 360° in Figure 7(B).

With the aforementioned electric-tweezer manipulation technique, multiple nanomotors have been efficiently assembled into various designed patterns, such as 1×3 and 2×2 arrays, and rotated simultaneously [Figure 7(C)].[15] The rotation is fully controllable in both speed and direction.

To test the possible highest speed of the nanomotors, Fan *et al.* increased the electric field by five times via the reduction of the electrode separation from 500 to 100 μm. The applied AC frequency is also optimized (30 kHz) for a 10-μm-long Au/Ni/Au nanowire in DI water. Furthermore, by leveraging the advantageous dependence of speed on E^2, the nanomotors can reach a speed of 1.8×10^4 rpm at 17 V and 30 kHz, reaching that of a jet engine.[15]

To test how small such nanomotors can be, Fan *et al.* further reduced the length of the nanorotors to 800- 900 nm (~165 nm in diameter) and the diameter of the Cr/Ni/Au nanodisks to 200 nm (106 nm in thickness). Such nanomotors have all dimensions less than 1 μm, and are among the smallest nanomotors that have been created [Figure 7(D)].[15] The length of the nanorotors was chosen to be just below 1 μm to be observable by optical microscopes. The feature size of the nanomotors can be much smaller than 1 μm, which is determined by the relative levels of the applied electric forces and the Brownian motion effect and need more investigation.

It is extremely difficult to operate micro/nanoscale actuators with long lifetime. Only a few of nanomotors have been able to continuously operate for a few hours.[19,138] Recently, it was demonstrated that nanomotors built from magnetic bearings with Au as the top layers can continuously rotate for 15 – 43 hours or over 240,000 – 500, 000 cycles in total.[15,55] With understanding of the interfacial wear problem at the contact point of the rotors and bearings, Ti was used as the top layer of the bearings replacing Au, which substantially enhanced the lifetime of the nanomotors to 80 hours over 1.1 million cycles [Figure 7(E)].[55] The improvement can be attributed to the higher resistance of Ti to abrasion and deformation compared to that of Au.

As shown in the torque analysis in Eq. (4), a simply designed nanomotor with the so-called chopstick magnetic configuration in Figure 7(A) and [Figure 7(F), i] rotated with oscillating rotation speed due to the magnetic torque between the magnetic segment in the nanowire

rotor and the magnetic Ni layer in the bearing. It is highly coveted to achieve nanomotors that can rotate with uniform speed and stop at arbitrary angular positions, like step motors. To address this need, nanoentities with different magnetic moments, orientations, and dimensions are assembled into nanomotors with designed magnetic configurations, such as the perpendicular configuration [Fig. 7(F), ii], where both the magnetic moments in the nanowire and bearings are perpendicular to the plane of rotation, and (ii) the T-shape configuration [Figure 7(F), iii], where the aforementioned magnetic moments are perpendicular to each other.[139] While the nanomotors with the chopstick configuration [Figure 7(F), i] have finite magnetic torque and force, given by $\tau_m = (\mu_0 m_1 m_2/4\pi x^3) \sin \Theta$ and $F_m = (3\mu_0 m_1 m_2/4\pi x^4) \cos\Theta$, respectively, which directly result in the periodic rotation speed, those for the perpendicular and T-shape configured nanomotors have zero or non-angle dependent magnetic torques of $\tau_m = 0$ or $\tau_m \propto \mu_0 m_1 m_2/\pi x^3$, respectively. Indeed, in experiments, uniform rotation speeds have been achieved from the perpendicular and T-shape configured nanomotors. The nanomotors can be positioned at arbitrary angles by the AC electric field, like step motors [Figure 7(F), iv].

3.3.1.5. Silicon Nanomotors: Silicon is one of the most widely used materials in microelectronics, energy devices, and MEMS due to its abundance on earth, compatibility with IC fabrication processes,[140] and rich physical properties.[141] Xu *et al.* demonstrated nanomotors made of Si nanowire rotors and revealed its unique actuation behaviors in electric fields.[137] The Si nanowire rotors were 200 nm in diameter and 7.3 – 14.4 μm in length, prepared via Ag assisted hydrofluoride etching through nanosphere masks. To assemble them into nanomotors, a 250-nm-thick Ni layer was deposited at the tips of the nanowires [Figure 8(A)]. By using the same manipulation and assembling techniques, *i.e.*, the electric tweezers and magnetic attraction, the first Si-based nanoscale rotary motors have been realized with fully controlled speed and orientation.

3.3.1.6. Tunable Biochemical Release: The electric nanomotors have been applied in tuning biochemical release rate by their mechanical rotation.[15,142] To detect the real-time release rate of molecules, plasmonic-active nanomotors were designed and fabricated, consisting of silica-coated Au/Ni/Au nanowires with Ag nanoparticles uniformly distributed on the surfaces [Figure 8(B)]. Various molecules, such as nile blue and R6-G were adsorbed in the silica layers on the surfaces. On such a structure, under illumination of laser, the intensity of Raman spectra of molecules in the hotspots at the junctions of the Ag nanoparticles can be substantially enhanced with E^4 dependence for real-time detection of molecules. This is the so-called Surface-Enhanced Raman Scattering (SERS). The enhancement factors are $10^9 – 10^{10}$, among the highest reported in literature.[143] It is observed that the release rate (k) of molecules monotonically increases with square root of rotation speed ($\sqrt{\omega}$). This quantitative dependence has been unveiled for the first time and can be understood by the fluidic boundary layer theory.[142] The new mechanism of controlled molecule release with mechanical rotations can be applied to all types of biomolecules, such as drugs, cytokine, DNA, antigens, and antibodies.

3.3.2. Synchronous Electrorotation—Different from the direct use of rotating electric field to drive nanoparticles, Edwards *et al.* employed electric fields comprised of two AC

signals with distinct frequencies to realize controlled rotation of nanowires. One AC signal was dedicated to the polarization of the nanowires (the high frequency AC signal) and the other AC signal compelled the rotation of nanoparticles (the low frequency modulation AC signal).[130] With such a configuration, nanowires were rotated at the same frequency with that of the low-frequency AC electric signal. The authors first explored the frequencies of the carrier signal required to effectively polarize nanowires. Nanowires were dispersed between a set of parallel electrodes. The alignment in a uniform AC electric field was observed when sweeping the frequency. It was found that nanowires (6 μm in length and 150 nm in diameter on average) were aligned at frequency above ~500 Hz. In the experiments, the carrier signal was set at 1 kHz, which was able to polarize even shorter nanowires in the suspension. To achieve continuous rotation of nanowires, along with the1 kHz carrier signal applied to quadruple microelectrodes with sequential 90° phase shifts, a modulation signal was applied with much lower frequencies (0 – 2 Hz). All the nanowires were rotating at a speed same as the modulation frequency regardless of the nanowire geometry, electric field intensity, liquid properties, or carrier signal frequency [Figure 8(C)]. Therefore, the rotation speed increased with the modulation frequency. At higher frequencies, however, the nanowires lost the synchrony and their rotation speed was reduced. This effect determined the maximum rotation speed, which was ~0.9 Hz for nanowires with an average length of 6 μm and diameter of 300 nm. While the highest speed is limited by the low-frequency AC signal, the synchronous rotation is advantageous in applications that require alignment of multiple nanowires of different geometry during rotation.

3.3.3. Chemically Driven Rotation of Conducting Objects Induced by Electric Fields—Besides catalytic motors, there is another type of chemical motors powered by electric field, called bipolar electrochemistry. Due to external electric fields, the polarization voltage induced along a conducting object can activate redox reactions. The induced polarization voltage ΔV is proportional to the electric field E and the dimension of object l (along the electric field direction), as given by equation (5):

$$\Delta V = El. \quad (5)$$

When ΔV is high enough, redox reaction takes place. The area where accumulated electrons reduce protons serves as the cathode, while the opposite area of the object where oxidation reaction takes place is the anode. The spatial separation of the reduction and oxidation reaction in bipolar electrochemistry has attracted much attention in different areas, especially in materials synthesis.[144–147] Now by exploiting this feature, locomotion of the conducting object can be achieved.

Loget and Kuhn's work has shown that both linear and rotatory motors can be designed by using bipolar electrochemistry.[148] For propulsion, water-splitting reaction induced at the anode and the cathode generates hydrogen and oxygen bubbles, respectively. Due to conservation of charges, the amount of hydrogen generated is twice as much as that of oxygen, which leads to an unbalanced propulsion force and thus drives the object to move with the anode area as the front.

Based on this concept, they also achieved rotary motion. The rotor was a carbon-doped polycarbonate cross supported by a thin glass needle axis. The rotation plane was either parallel or perpendicular to the bottom of the cell [Figure 9(A)]. Most of the cross surface was shielded by the insulating polymer [blue area in Figure 9(A)] except the extremities [red area in Figure 9(A)]. By imposing an electric field of 0.5 kV m− 1, corresponding to a ΔV of 8.5 V, water-splitting reaction was induced at the extremities of the object. Bubbles generated on both anode and cathode produced torque to rotate the cross counterclockwise. Once the conducting part pass through the virtual plane, it reversed the polarization direction, thus the anode and cathode also commuted and kept the rotation continuous. An average rotational speed of 1.9° s^{-1} has been achieved on a horizontal motor. As for the rotation in vertical plane, the buoyant force of the gas bubbles also contributed to the rotational torque. To further enhance the rotational speed, the generation of O_2 was suppressed by adding hydroquinone and the rotor was designed in a way that H_2 bubbles were always generated below the rotor blade and attached to the surface. An average rotation speed of 4.2° s^{-1} was obtained from a vertical motor, which was more than twice higher than that of the horizontal motor.

This type of motors is advantageous in the versatility of materials selection compared to the aforediscussed catalytic motors. Presently, the demonstrated devices are in a centimeter to millimeter range. To achieve manipulations of smaller devices, electric field could be increased according to Eq. (6).

3.3.4. Magnetic-Domain-Wall Mediated Rotation of Nanospheres Controlled by Electric Fields—Sohn *et al.* experimentally demonstrated rotation of magnetic particles via manipulating magnetic domain walls controlled by electric fields [Figure 9(B)].[149] First, ferromagnetic Ni rings (outer diameters of 1 – 4 μm, width of 150 – 800 nm, and thickness of 15 – 45 nm) were fabricated on piezoelectric substrates $[Pb(Mg_{1/3}Nb_{2/3})O_3]_{0.66}$–$[PbTiO_3]0.34$ (PMN–PT) and magnetized with a 3 kOe external magnetic field. Depending on the dimensions, magnetic rings formed different magnetic domain wall structures.[150,151] “Onion” state, which has two magnetic domains parallel to each other on each side of a Ni ring [Figure 9(B)], were created from 30-nm-thick Ni rings with a width/outer diameter ratio ≤ 0.3 and all 15-nm-thick Ni rings. When an electric field was applied, the PMN-PT substrates induced compressive strain in the [100] direction and tensile strain in the $[01\ \bar{1}]$ direction, which drove the domain walls to rotate 45° to the [100] direction due to the magnetostriction effect of Ni. By tuning on and off the electric field, the domain walls can be rotated reciprocally. As a result, superparamagnetic microbeads (SPMs: 1 μm in diameter) attached to the domain walls can rotate synchronously.

3.4. Acoustic Micro/Nanomotors

Acoustic propulsion of micro/nanoentities has recently come into the spotlight as a promising candidate for micro/nanomanipulation with many applications in biological systems. This type of micro/nanomachine converts acoustic energy transmitted in a form of ultrasonic waves into mechanical motion. Ultrasound has been widely used for medical applications such as noninvasive imaging and physical therapy and proven harmless to human body and biocompatible.[152,153] It does not require toxic chemicals or harmful

materials and can effectively drive micro/nanoparticles with large thrust output in a wide range of working conditions including high-viscosity or high-ionic strength media.[154–156] Moreover, in conjunction with other techniques such as magnetic tweezers, it is possible to remotely control the motion of acoustic nanomachines, which is essential for biomedical applications.[157] Although, up to date, most ultrasonic micro/nanomachines are based on translational motion for conveying,[154,155,158,159] arranging,[160–162] and sorting[163,164] particles, microorganisms, and biomolecules, some of them can effectively drive micro/nanoentities to rotate.

Shilton *et al.* used surface acoustic waves (SAWs) to drive millimeter-scale disc rotors [Figure 10(A)].[165] SAWs were generated with a set of interdigital transducers (IDTs) patterned on a piezoelectric substrate and transmitted to a water droplet from each side in opposite directions. Silicone dampers were asymmetrically placed on the pathways of the SAWs and let each SAW reach only one half of the droplet or the other, respectively. This asymmetry resulted in a rotating flow of the droplet, and a 5-mm-diameter mylar disc floating on the droplet can be rotated. Its rotation speed was controlled with the electrical input power up to 2250 rpm with maximum torque of 60 nN·m.

In the work on self-acoustophoretic propulsion of nanoentities, Wang *et al.* reported different types of motion from the nanoentities including translation, pattern formation, orbital revolution, and axial rotation [Figure 10(B)].[154] When an acoustic field was applied from the bottom at a certain frequency, a standing wave was formed between a stainless steel plate cell bottom and a cover slip. Metal nanorods suspended in a liquid medium were levitated to a nodal plane which has the minimum acoustic pressure. The acoustic wave was scattered at the surface of the nanorods and created acoustic pressure gradients around them. Depending on the acoustic field gradient, nanorods showed different behavior. Among those, a helical acoustic wave drove nanorods rotate either around the long axis or along an orbital path on the nodal plane. In the following work, self-acoustophoretic nanomotors were demonstrated with living cells. HeLa cells with Au nanomotors attached on the surface can be chained and rotated in acoustic fields [Figure 10(C)].[159] In another work, Balk *et al.* visualized the axial rotation of metal nanorods in an acoustic field with polystyrene nanoparticles serving as optical tracers and revealed that the nanorods rotated around their long axis at ~150 000 rpm.[14]

Huang's group recently developed polymer micromotors driven by oscillating bubbles in an acoustic field.[156] They fabricated hydrophobic polymer blocks with cavities using photo-curable polyethylene glycol (PEG) mixture. When the blocks were suspended in a liquid medium, tiny bubbles formed inside the cavities. They were oscillated with an acoustic wave and generated a steady flow field around the polymer microblocks, which provided thrust. The polymer microblocks moved in different modes depending on the size, location, and number of bubbles trapped in the cavities. Those with asymmetric bubbles, *e.g.*, an off-centered single bubble or multiple bubbles with different sizes, can rotate in an acoustic field [Figure 10(D)].

4. Discussion/perspectives/conclusion

With intensive research efforts, significant progresses have been achieved in developing rotary nanomotors. In this work, we reviewed the concepts, working mechanisms, design, fabrication, and applications of various synthetic rotary nanomotors. The performance of nanomotors has been improved significantly in terms of control, speed, and lifetime. While early research focused on conceptual demonstration of each type of nanomotor, more research has been carried out recently on their practical applications such as tuning of biochemical release[15] and cargo delivery.[4–6]

Despite remarkable progresses, rotary nanomotors still have many unmet challenges to overcome before they can practically benefit in our daily lives. First of all, to be used as nanomachines for biomedical applications, such as nanoscale surgery,[166] drug delivery,[167] and cell study,[168] nanomotors should be biocompatible in both the employed constitute materials and energy sources. Most of the aforementioned nanomotors consist of synthetic materials, some of which are toxic metals to live cells. Certain energy sources are corrosive, toxic, unavailable in natural biological systems, or cannot be easily delivered to live beings. In this context, it is essential to investigate new materials, actuation mechanisms, and energy delivery device of nanomotors. Along with the biocompatibility issue, how to deliver nanomachines into living organisms across various barriers, to provide them with sufficient power, to remotely control their motion, and to receive their transmitted signals should be investigated. Second, a large number rotary nanomachines that have been reported are simply free rotating nanoparticles in suspension that cannot deliver forces or torques effectively. It is extremely important to explore innovative designs and the associated assembling techniques to realize sophisticated nanomachines that can operate cooperatively at fixed positions for meaningful and useful functions, such as sorting and probing biological cells. Third, most reported rotary nanomotors are made of simple materials and structures, such as Au nanowires. To be functional, *i.e.*, for sensing and actuation, it is critical to design nanomotors with more sophisticated materials, morphologies, and structures.[15,142] In this context, the designing and fabrication of structural and functional micro/nanoswimmers, such as chiral micro/nanoswimmers and SERS-active nanomotors, can represent an important future direction of micro/nanomachines. One important goal in nanomotor research is to equip nanomachines with intelligence so that they can simultaneously sense surroundings and make actuations based on the sensing results. Fourth, it is of great interest to manipulate individual rotary nanomotors amidst many as well as to drive a swarm of nanomotors. Each type of manipulation has its own importance and perspective applications. Overall, continuous development and progress of nanomotors are exciting and critical for the future intelligent nanorobots and nanofactories, which have been dreamed of and will have huge impact on our lives.

Acknowledgments

This work is supported by National Science Foundation (CAREER Award Grant No. CMMI 1150767 and ECCS-1446489), Welch Foundation (Grant No. F-1734), and National Institutes of Health (9R42ES024023-02) in part. Jianhe Guo thanks Howard Hughes Medical Institute for the International Student Research Fellowship.

References

1. Feynman RP. Eng Sci. 1960; 23:22–36.
2. Ozin GA, Manners I, Fournier-Bidoz S, Arsenault A. Adv Mater. 2005; 17:3011–3018.
3. Wang H, Pumera M. Chem Rev. 2015; 115:8704–8735. [PubMed: 26234432]
4. Sundararajan S, Lammert P, Zudans A, Crespi V, Sen A. Nano Lett. 2008; 8:1271–1276. [PubMed: 18416540]
5. Burdick J, Laocharoensuk R, Wheat PM, Posner JD, Wang J. J Am Chem Soc. 2008; 130:8164–8165. [PubMed: 18533716]
6. Wang J. Lab Chip. 2012; 12:1944–1950. [PubMed: 22395152]
7. Guix M, Mayorga-Martinez CC, Merkoçi A. Chem Rev. 2014; 114:6285–6322. [PubMed: 24827167]
8. Fan D, Yin Z, Cheong R, Zhu FQ, Cammarata RC, Chien CL, Levchenko A. Nat Nanotechnol. 2010; 5:545–551. [PubMed: 20543835]
9. Gao W, Kagan D, Pak OS, Clawson C, Campuzano S, Chuluun-Erdene E, Shipton E, Fullerton EE, Zhang L, Lauga E, Wang J. 2012; 8:460–467.
10. Campuzano S, Kagan D, Orozco J, Wang J. Analyst. 2011; 136:4621–4630. [PubMed: 21915400]
11. Xu X, Li H, Hasan D, Ruoff RS, Wang AX, Fan DL. Adv Funct Mater. 2013; 23:4332–4338.
12. Hanay MS, Kelber S, Naik AK, Chi D, Hentz S, Bullard EC, Colinet E, Duraffourg L, Roukes ML. Nat Nanotechnol. 2012; 7:602–608. [PubMed: 22922541]
13. Gultepe E, Randhawa JS, Kadam S, Yamanaka S, Selaru FM, Shin EJ, Kalloo AN, Gracias DH. Adv Mater. 2012; 25:514–519. [PubMed: 23047708]
14. Balk AL, Mair LO, Mathai PP, Patrone PN, Wang W, Ahmed S, Mallouk TE, Liddle JA, Stavis SM. ACS Nano. 2014; 8:8300–8309. [PubMed: 25019966]
15. Kim K, Xu X, Guo J, Fan DL. Nat Commun. 2014; 5:3632. [PubMed: 24709694]
16. Liu M, Zentgraf T, Liu Y, Bartal G, Zhang X. Nat Nanotechnol. 2010; 5:570–573. [PubMed: 20601945]
17. Ghosh A, Fischer P. Nano Lett. 2009; 9:2243–2245. [PubMed: 19413293]
18. Qin L, Banholzer MJ, Xu X, Huang L, Mirkin CA. J Am Chem Soc. 2007; 129:14870–14871. [PubMed: 17988136]
19. Frechette LG, Nagle SF, Ghodssi R, Umans SD, Schmidt MA, Lang JH. IEEE. 2001:290–293.
20. Ghalichechian N, Modafe A, Beyaz MI, Ghodssi R. J Microelectromech Syst. 2008; 17:632–642.
21. Soong RK, Bachand GD, Neves HP, Olkhovets AG, Craighead HG, Montemagno CD. Science. 2000; 290:1555–1558. [PubMed: 11090349]
22. Bhushan, B., editor. Tribology issues and opportunities in MEMS. Kluwer Academic Publishers; Dordrecht; Boston: 1998.
23. Paxton WF, Sen A, Mallouk TE. Chem Eur J. 2005; 11:6462–6470. [PubMed: 16052651]
24. Cao, G.; Wang, Y. Nanostructures and nanomaterials: synthesis, properties, and applications. World Scientific; Singapore; London: 2011.
25. Xia Y, Yang P, Sun Y, Wu Y, Mayers B, Gates B, Yin Y, Kim F, Yan H. Adv Mater. 2003; 15:353–389.
26. Fennimore AM, Yuzvinsky TD, Han WQ, Fuhrer MS, Cumings J, Zettl A. Nature. 2003; 424:408–410. [PubMed: 12879064]
27. Schnitzer MJ, Block SM. Nature. 1997; 388:386–390. [PubMed: 9237757]
28. Kitamura K, Tokunaga M, Iwane AH, Yanagida T. Nature. 1999; 397:129–134. [PubMed: 9923673]
29. Wang MD, Schnitzer MJ, Yin H, Landick R, Gelles J, Block SM. Science. 1998; 282:902–907. [PubMed: 9794753]
30. Noji H, Yasuda R, Yoshida M, Kinosita K Jr. Nature. 1997; 386:299–302. [PubMed: 9069291]
31. Montemagno C, Bachand G. Nanotechnology. 1999; 10:225–231.

32. Tsunoda SP, Aggeler R, Yoshida M, Capaldi RA. Proc Natl Acad Sci USA. 2001; 98:898–902. [PubMed: 11158567]
33. Mano N, Heller A. J Am Chem Soc. 2005; 127:11574–11575. [PubMed: 16104713]
34. Di Leonardo R, Angelani L, Dell'Arciprete D, Ruocco G, Iebba V, Schippa S, Conte MP, Mecarini F, De Angelis F, Di Fabrizio E. Proc Natl Acad Sci USA. 2010; 107:9541–9545. [PubMed: 20457936]
35. Paxton WF, Kistler KC, Olmeda CC, Sen A, St Angelo SK, Cao Y, Mallouk TE, Lammert PE, Crespi VH. J Am Chem Soc. 2004; 126:13424–13431. [PubMed: 15479099]
36. Fournier-Bidoz S, Arsenault AC, Manners I, Ozin GA. Chem Commun. 2005:441–443.
37. Kagan D, Calvo-Marzal P, Balasubramanian S, Sattayasamitsathit S, Manesh K, Flechsig G, Wang J. J Am Chem Soc. 2009; 131:12082–12083. [PubMed: 19670862]
38. Valadares L, Tao Y, Zacharia N, Kitaev V, Galembeck F, Kapral R, Ozin G. 2010; 6:565–572.
39. Gibbs JG, Zhao YP. Appl Phys Lett. 2009; 94:163104.
40. Gao W, Pei A, Wang J. ACS Nano. 2012; 6:8432–8438. [PubMed: 22891973]
41. Mou F, Chen C, Ma H, Yin Y, Wu Q, Guan J. Angew Chem Int Ed. 2013; 52:7208–7212.
42. Gao W, Uygun A, Wang J. J Am Chem Soc. 2012; 134:897–900. [PubMed: 22188367]
43. Laocharoensuk R, Burdick J, Wang J. ACS Nano. 2008; 2:1069–1075. [PubMed: 19206505]
44. Liu R, Sen A. J Am Chem Soc. 2011; 133:20064–20067. [PubMed: 21961523]
45. Wang S, Wu N. Langmuir. 2014; 30:3477–3486. [PubMed: 24593832]
46. Catchmark JM, Subramanian S, Sen A. 2005; 1:202–206.
47. Wang Y, Fei ST, Byun YM, Lammert PE, Crespi VH, Sen A, Mallouk TE. J Am Chem Soc. 2009; 131:9926–9927. [PubMed: 19572715]
48. Vicario J, Eelkema R, Browne WR, Meetsma A, La Crois RM, Feringa BL. Chem Commun. 2005:3936–3938.
49. He Y, Wu J, Zhao Y. Nano Lett. 2007; 7:1369–1375. [PubMed: 17430007]
50. Gibbs JG, Zhao YP. 2009; 5:2304–2308.
51. Gibbs JG, Zhao Y. 2010; 6:1656–1662.
52. Gibbs JG, Fischer P. Chem Commun. 2015; 51:4192–4195.
53. Solovev AA, Xi W, Gracias DH, Harazim SM, Deneke C, Sanchez S, Schmidt OG. ACS Nano. 2012; 6:1751–1756. [PubMed: 22233271]
54. Liu W, He R, Zhu H, Hu H, Li M, Zhao XZ. Appl Phys Lett. 2010; 96:053114.
55. Guo J, Kim K, Lei KW, Fan DL. Nanoscale. 2015; 7:11363–11370. [PubMed: 26073977]
56. Crick FHC, Hughes AFW. Exp Cell Research. 1950; 1:37–80.
57. Ryu KS, Shaikh K, Goluch E, Fan Z, Liu C. Lab Chip. 2004; 4:608–613. [PubMed: 15570373]
58. Köhler J, Ghadiri R, Ksouri SI, Guo Q, Gurevich EL, Ostendorf A. J Phys D: Appl Phys. 2014; 47:505501.
59. Strick TR, Allemand JF, Bensimon D, Bensimon A, Croquette V. Science. 1996; 271:1835–1837. [PubMed: 8596951]
60. Mosconi F, Allemand JF, Bensimon D, Croquette V. Phys Rev Lett. 2009; 102:078301. [PubMed: 19257716]
61. Celedon A, Nodelman IM, Wildt B, Dewan R, Searson P, Wirtz D, Bowman GD, Sun SX. Nano Lett. 2009; 9:1720–1725. [PubMed: 19301859]
62. Lipfert J, Kerssemakers JWJ, Jager T, Dekker NH. Nat Methods. 2010; 7:977–980. [PubMed: 20953173]
63. Lipfert J, Wiggin M, Kerssemakers JWJ, Pedaci F, Dekker NH. Nat Commun. 2011; 2:439. [PubMed: 21863006]
64. Lipfert J, Kerssemakers JJW, Rojer M, Dekker NH. Rev Sci Instrum. 2011; 82:103707. [PubMed: 22047303]
65. De Vlaminck I, Dekker C. Annu Rev Biophys. 2012; 41:453–472. [PubMed: 22443989]
66. Tanase M, Felton EJ, Gray DS, Hultgren A, Chen CS, Reich DH. Lab Chip. 2005; 5:598–605. [PubMed: 15915251]

67. Sniadecki NJ, Anguelouch A, Yang MT, Lamb CM, Liu Z, Kirschner SB, Liu Y, Reich DH, Chen CS. Proc Natl Acad Sci USA. 2007; 104:14553–14558. [PubMed: 17804810]
68. Ishiyama K, Sendoh M, Yamazaki A, Arai KI. Sens Actuators A. 2001; 91:141–144.
69. Ishiyama K, Sendoh M, Arai KI. J Magn Magn Mater. 2002; 242–245:41–46.
70. Zhang L, Abbott JJ, Dong L, Kratochvil BE, Bell D, Nelson BJ. Appl Phys Lett. 2009; 94:064107.
71. Zhang L, Abbott JJ, Dong L, Peyer KE, Kratochvil BE, Zhang H, Bergeles C, Nelson BJ. Nano Lett. 2009; 9:3663–3667. [PubMed: 19824709]
72. Zhang L, Peyer KE, Nelson BJ. Lab Chip. 2010; 10:2203–2215. [PubMed: 20567752]
73. Tottori S, Zhang L, Qiu F, Krawczyk KK, Franco-Obregón A, Nelson BJ. Adv Mater. 2012; 24:811–816. [PubMed: 22213276]
74. LaFratta CN, Fourkas JT, Baldacchini T, Farrer RA. Angew Chem Int Ed. 2007; 46:6238–6258.
75. Tottori S, Zhang L, Peyer KE, Nelson BJ. Nano Lett. 2013; 13:4263–4268. [PubMed: 23947427]
76. Hawkeye MM, Brett MJ. J Vac Sci Technol A. 2007; 25:1317–1335.
77. Ghosh A, Paria D, Singh HJ, Venugopalan PL, Ghosh A. Phys Rev E. 2012; 86:031401.
78. Venugopalan PL, Sai R, Chandorkar Y, Basu B, Shivashankar S, Ghosh A. Nano Lett. 2014; 14:1968–1975. [PubMed: 24641110]
79. Schamel D, Mark AG, Gibbs JG, Miksch C, Morozov KI, Leshansky AM, Fischer P. ACS Nano. 2014; 8:8794–8801. [PubMed: 24911046]
80. Walker D, Kübler M, Morozov KI, Fischer P, Leshansky AM. Nano Lett. 2015; 15:4412–4416. [PubMed: 26030270]
81. Liu L, Yoo SH, Lee SA, Park S. Nano Lett. 2011; 11:3979–3982. [PubMed: 21819102]
82. Li J, Sattayasamitsathit S, Dong R, Gao W, Tam R, Feng X, Ai S, Wang J. Nanoscale. 2014; 6:9415–9420. [PubMed: 24126904]
83. Gao W, Feng X, Pei A, Kane CR, Tam R, Hennessy C, Wang J. Nano Lett. 2014; 14:305–310. [PubMed: 24283342]
84. Gao W, Sattayasamitsathit S, Manesh KM, Weihs D, Wang J. J Am Chem Soc. 2010; 132:14403–14405. [PubMed: 20879711]
85. Tierno P, Golestanian R, Pagonabarraga I, Sagués F. Phys Rev Lett. 2008; 101:218304. [PubMed: 19113458]
86. Tierno P, Golestanian R, Pagonabarraga I, Sagués F. J Phys Chem B. 2008; 112:16525–16528. [PubMed: 19367983]
87. Tierno P, Güell O, Sagués F, Golestanian R, Pagonabarraga I. Phys Rev E. 2010; 81:011402.
88. Sing CE, Schmid L, Schneider MF, Franke T, Alexander-Katz A. Proc Natl Acad Sci USA. 2010; 107:535–540. [PubMed: 20080716]
89. Zhang L, Petit T, Lu Y, Kratochvil B, Peyer K, Pei R, Lou J, Nelson B. ACS Nano. 2010; 4:6228–6234. [PubMed: 20873764]
90. Zhang L, Petit T, Peyer KE, Nelson BJ. Nanomedicine. 2012; 8:1074–1080. [PubMed: 22426194]
91. Xi W, Solovev AA, Ananth AN, Gracias DH, Sanchez S, Schmidt OG. Nanoscale. 2013; 5:1294–1297. [PubMed: 23154823]
92. Ashkin A, Dziedzic JM, Bjorkholm JE, Chu S. Opt Lett. 1986; 11:288–290. [PubMed: 19730608]
93. Sato S, Ishigure M, Inaba H. Electron Lett. 1991; 27:1831–1832.
94. O'Neil AT, Padgett MJ. Opt Lett. 2002; 27:743–745. [PubMed: 18007918]
95. Dasgupta R, Mohanty SK, Gupta PK. Biotechnol Lett. 2003; 25:1625–1628. [PubMed: 14584918]
96. Forrester A, Courtial J, Padgett MJ. J Mod Opt. 2003; 50:1533–1538.
97. Maruo S, Inoue H. Appl Phys Lett. 2007; 91:084101.
98. Beth R. Phys Rev. 1936; 50:115–125.
99. Friese MEJ, Nieminen TA, Heckenberg NR, Rubinsztein-Dunlop H. Nature. 1998; 394:348–350.
100. Friese MEJ, Rubinsztein-Dunlop H, Gold J, Hagberg P, Hanstorp D. Appl Phys Lett. 2001; 78:547–549.
101. He H, Friese MEJ, Heckenberg NR, Rubinsztein-Dunlop H. Phys Rev Lett. 1995; 75:826–829. [PubMed: 10060128]

102. Friese MEJ, Enger J, Rubinsztein-Dunlop H, Heckenberg NR. Phys Rev A. 1996; 54:1593–1596. [PubMed: 9913630]
103. Simpson NB, Dholakia K, Allen L, Padgett MJ. Opt Lett. 1997; 22:52–54. [PubMed: 18183100]
104. Paterson L, MacDonald MP, Arlt J, Sibbett W, Bryant PE, Dholakia K. Science. 2001; 292:912–914. [PubMed: 11340200]
105. Curtis JE, Grier DG. Phys Rev Lett. 2003; 90:133901. [PubMed: 12689289]
106. O'Neil AT, Padgett MJ. Opt Commun. 2000; 185:139–143.
107. Grier DG. Nature. 2003; 424:810–816. [PubMed: 12917694]
108. Lin XF, Hu GQ, Chen QD, Niu LG, Li QS, Ostendorf A, Sun HB. Appl Phys Lett. 2012; 101:113901.
109. Padgett M, di Leonardo R. Lab Chip. 2011; 11:1196–1205. [PubMed: 21327211]
110. Curtis JE, Koss BA, Grier DG. Opt Commun. 2002; 207:169–175.
111. Leach J, Mushfique H, di Leonardo R, Padgett M, Cooper J. Lab Chip. 2006; 6:735–739. [PubMed: 16738723]
112. Ladavac K, Grier DG. Opt Express. 2004; 12:1144–1149. [PubMed: 19474932]
113. Higurashi E, Ukita H, Tanaka H, Ohguchi O. Appl Phys Lett. 1994; 64:2209–2210.
114. Higurashi E, Ohguchi O, Tamamura T, Ukita H, Sawada R. J Appl Phys. 1997; 82:2773–2779.
115. Galajda P, Ormos P. Appl Phys Lett. 2001; 78:249–251.
116. Galajda P, Ormos P. Appl Phys Lett. 2002; 80:4653–4655.
117. Maruo S, Takaura A, Saito Y. Opt Express. 2009; 17:18525–18532. [PubMed: 20372583]
118. Lin CL, Vitrant G, Bouriau M, Casalegno R, Baldeck PL. Opt Express. 2011; 19:8267–8276. [PubMed: 21643076]
119. Schuller JA, Barnard ES, Cai W, Jun YC, White JS, Brongersma ML. Nat Mater. 2010; 9:193–204. [PubMed: 20168343]
120. Wang K, Schonbrun E, Steinvurzel P, Crozier KB. Nat Commun. 2011; 2:469. [PubMed: 21915111]
121. Shao L, Yang ZJ, Andrén D, Johansson P, Käll M. ACS Nano. 2015; 9:12542–12551. [PubMed: 26564095]
122. Jones PH, Palmisano F, Bonaccorso F, Gucciardi PG, Calogero G, Ferrari AC, Maragó OM. ACS Nano. 2009; 3:3077–3084. [PubMed: 19856981]
123. Zong Y, Liu J, Liu R, Guo H, Yang M, Li Z, Chen K. ACS Nano. 2015; 9:10844–10851. [PubMed: 26481901]
124. Liaw JW, Chen YS, Kuo MK. Opt Express. 2014; 22:26005. [PubMed: 25401634]
125. Yan Z, Scherer NF. J Phys Chem Lett. 2013; 4:2937–2942.
126. Yan Z, Sweet J, Jureller JE, Guffey MJ, Pelton M, Scherer NF. ACS Nano. 2012; 6:8144–8155. [PubMed: 22900883]
127. Moocarme M, Kusin B, Vuong LT. Opt Mater Express. 2014; 4:2355–2367.
128. Fan DL, Zhu FQ, Cammarata RC, Chien CL. Phys Rev Lett. 2005; 94:247208.
129. Fan DL, Zhu FQ, Cammarata RC, Chien CL. Nano Today. 2011; 6:339–354.
130. Edwards B, Mayer TS, Bhiladvala RB. Nano Lett. 2006; 6:626–632. [PubMed: 16608256]
131. Xu X, Kim K, Li H, Fan DL. Adv Mater. 2012; 24:5457–5463. [PubMed: 22887635]
132. Fan DL, Zhu FQ, Cammarata RC, Chien CL. Appl Phys Lett. 2004; 85:4175–4177.
133. Whitney TM, Searson PC, Jiang JS, Chien CL. Science. 1993; 261:1316–1319. [PubMed: 17731862]
134. Fan DL, Cammarata RC, Chien CL. Appl Phys Lett. 2008; 92:093115.
135. Jones, TB. Electromechanics of particles. Cambridge University Press; Cambridge; New York: 1995.
136. Fan DL, Zhu FQ, Xu X, Cammarata RC, Chien CL. Proc Natl Acad Sci USA. 2012; 109:9309–9313. [PubMed: 22645373]
137. Xu X, Liu C, Kim K, Fan DL. Adv Funct Mater. 2014; 24:4843–4850.

138. Frechette LG, Jacobson SA, Breuer KS, Ehrich FF, Ghodssi R, Khanna R, Wong CW, Zhang X, Schmidt MA, Epstein AH. J Microelectromech Syst. 2005; 14:141–152.
139. Kim K, Guo J, Xu X, Fan DE. ACS Nano. 2015; 9:548–554. [PubMed: 25536023]
140. Lindroos, V.; Tilli, M.; Lehto, A.; Motooka, T. Handbook of Silicon Based MEMS Materials and Technologies. Elsevier; 2010.
141. Tang DM, Ren CL, Wang MS, Wei X, Kawamoto N, Liu C, Bando Y, Mitome M, Fukata N, Golberg D. Nano Lett. 2012; 12:1898–1904. [PubMed: 22435880]
142. Xu X, Kim K, Fan D. Angew Chem Int Ed. 2015; 54:2525–2529.
143. Xu X, Kim K, Liu C, Fan D. Sensors. 2015; 15:10422–10451. [PubMed: 25946633]
144. Loget G, Kuhn A. Anal Bioanal Chem. 2011; 400:1691–1704. [PubMed: 21455656]
145. Warakulwit, Chompunuch; Nguyen, Thi; Majimel, Jérome; Delville, Marie-Hélène; Lapeyre, Véronique; Garrigue, Patrick; Ravaine, Valérie; Limtrakul, A Jumras; Kuhn, Alexander. Nano Lett. 2008; 8:500–504. [PubMed: 18189438]
146. Loget G, Lapeyre V, Garrigue P, Warakulwit C, Limtrakul J, Delville MH, Kuhn A. Chem Mater. 2011; 23:2595–2599.
147. Bradley JC, Chen HM, Crawford J, Eckert J, Ernazarova K, Kurzeja T, Lin M, McGee M, Nadler W, Stephens SG. Nature. 1997; 389:268–271.
148. Loget G, Kuhn A. Nat Commun. 2011; 2:535. [PubMed: 22086336]
149. Sohn H, Nowakowski ME, Liang CY, Hockel JL, Wetzlar K, Keller S, McLellan BM, Marcus MA, Doran A, Young A, Kläui M, Carman GP, Bokor J, Candler RN. ACS Nano. 2015; 9:4814–4826. [PubMed: 25906195]
150. Zhu FQ, Chern GW, Tchernyshyov O, Zhu XC, Zhu JG, Chien CL. Phys Rev Lett. 2006; 96:027205. [PubMed: 16486626]
151. Zhu FQ, Fan D, Zhu X, Zhu JG, Cammarata RC, Chien CL. Adv Mater. 2004; 16:2155–2159.
152. Litvak E, Foster KR, Repacholi MH. Bioelectromagnetics. 2001; 23:68–82. [PubMed: 11793407]
153. Ziskin MC, Petitti DB. Ultrasound in Medicine and Biology. 1988; 14:91–96. [PubMed: 3279694]
154. Wang W, Castro LA, Hoyos M, Mallouk TE. ACS Nano. 2012; 6:6122–6132. [PubMed: 22631222]
155. Garcia-Gradilla V, Orozco J, Sattayasamitsathit S, Soto F, Kuralay F, Pourazary A, Katzenberg A, Gao W, Shen Y, Wang J. ACS Nano. 2013; 7:9232–9240. [PubMed: 23971861]
156. Ahmed D, Lu M, Nourhani A, Lammert PE, Stratton Z, Muddana HS, Crespi VH, Huang TJ. Sci Rep. 2015; 5:9744. [PubMed: 25993314]
157. Ahmed S, Wang W, Mair LO, Fraleigh RD, Li S, Castro LA, Hoyos M, Huang TJ, Mallouk TE. Langmuir. 2013; 29:16113–16118. [PubMed: 24345038]
158. Ding X, Lin SCS, Kiraly B, Yue H, Li S, Chiang IK, Shi J, Benkovic SJ, Huang TJ. Proc Natl Acad Sci USA. 2012; 109:11105–11109. [PubMed: 22733731]
159. Wang W, Li S, Mair L, Ahmed S, Huang TJ, Mallouk TE. Angew Chem Int Ed. 2014; 53:3201–3204.
160. Shi J, Ahmed D, Mao X, Lin SCS, Lawit A, Huang TJ. Lab Chip. 2009; 9:2890–2895. [PubMed: 19789740]
161. Chen Y, Ding X, Steven Lin S-C, Yang S, Huang P-H, Nama N, Zhao Y, Nawaz AA, Guo F, Wang W, Gu Y, Mallouk TE, Huang TJ. ACS Nano. 2013; 7:3306–3314. [PubMed: 23540330]
162. Guo F, Li P, French JB, Mao Z, Zhao H, Li S, Nama N, Fick JR, Benkovic SJ, Huang TJ. Proc Natl Acad Sci USA. 2015; 112:43–48. [PubMed: 25535339]
163. Ding X, Peng Z, Lin SCS, Geri M, Li S, Li P, Chen Y, Dao M, Suresh S, Huang TJ. Proc Natl Acad Sci USA. 2014; 111:12992–12997. [PubMed: 25157150]
164. Li P, Mao Z, Peng Z, Zhou L, Chen Y, Huang PH, Truica CI, Drabick JJ, El-Deiry WS, Dao M, Suresh S, Huang TJ. Proc Natl Acad Sci USA. 2015; 112:4970–4975. [PubMed: 25848039]
165. Shilton RJ, Glass NR, Chan P, Yeo LY, Friend JR. Appl Phys Lett. 2011; 98:254103.
166. Nelson BJ, Kaliakatsos IK, Abbott JJ. Annu Rev Biomed Eng. 2010; 12:55–85. [PubMed: 20415589]

167. Gao W, Wang J. Nanoscale. 2014; 6:10486–10494. [PubMed: 25096021]
168. Zhang L, Wang X. J Phys Chem Lett. 2015; 6:2530–2537. [PubMed: 26266730]

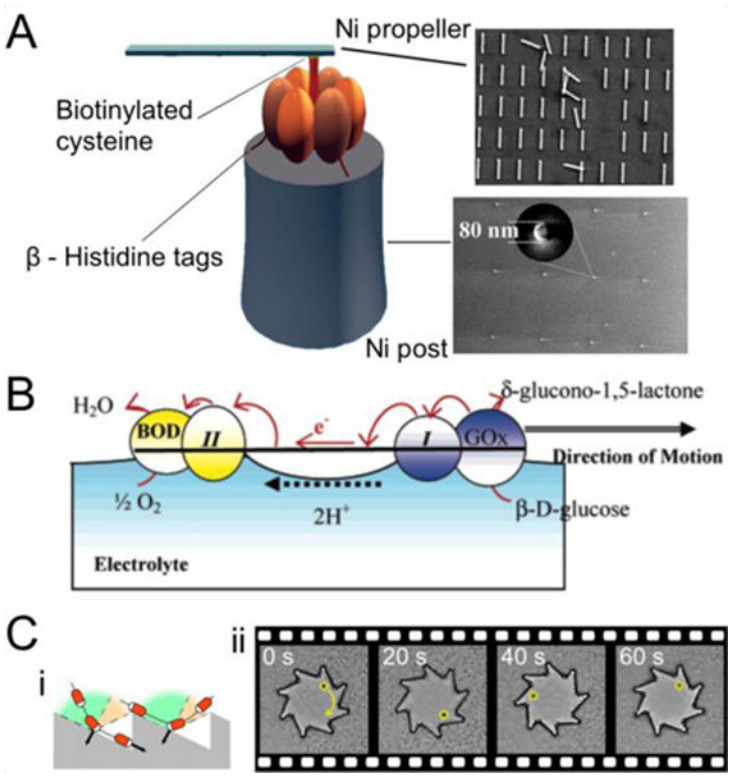

Figure 1. Bio-inorganic hybrid nanomachines

(A) A rotary nanomotor comprised of a molecular motor, a Ni propeller, and a Ni post. From Ref. [21]. Reprinted with permission from AAAS. (B) Illustration of a bioelectrochemical motor with bilirubin oxidase (BOD) and glucose oxidase (GOx) at each end of a conducting carbon fiber. Reprinted with permission from Ref. [33]. Copyright 2005 American Chemical Society. (C) Ratchet microgears driven by microorganisms: (i) an illustration of the collision and sliding of the microorganisms on gears and (ii) sequential micrographs showing the rotation of a microgear. Reproduced with permission from Ref. [34].

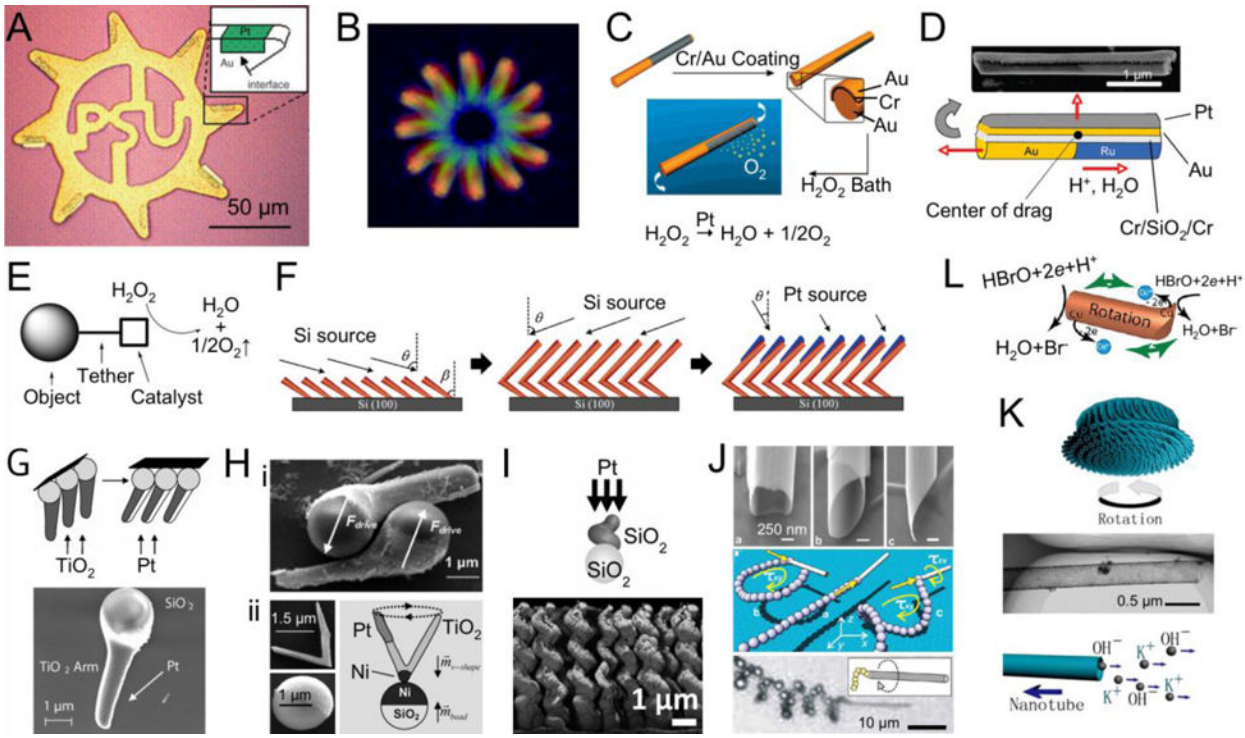

Figure 2. Catalytic motors

(A) Au microgear with Pt deposited on the steep side of the teeth. Reproduced with permission from Ref. [46]. Copyright 2005, Wiley-VCH. (B) Overlaid sequential micrographs of a rotating Au/Ni nanorod. Reproduced from Ref. [36] with permission from The Royal Society of Chemistry. (C) Structure and motion of rotating catalytic nanomotors composed of a Au/Pt/Au nanorod partially coated with Cr/Au. Reprinted with permission from Ref. [18]. Copyright 2007 American Chemical Society. (D) SEM image and a schematic diagram of aPt/Au/Cr/SiO_2/Cr-coated Au/Ru catalytic nanomotor rotating around its center. Reprinted with permission from Ref. [47]. Copyright 2009 American Chemical Society. (E) Catalytic motors with a silica bead tethered to a synthetic manganese catalase. Reproduced from Ref. [48] with permission from The Royal Society of Chemistry. (F) Dynamic shadowing growth (DSG) of the L-shaped Si/Pt catalytic motors. Reprinted with permission from Ref. [49]. Copyright 2007 American Chemical Society. (G) Nanomotors with SiO_2 heads and Pt-coated TiO_2 arms. Reproduced with permission from Ref. [50]. Copyright 2009, Wiley-VCH. (H) Self-assembled catalytic nanomotors with (i) two tadpoles consisting of SiO_2 heads and Pt-coated TiO_2 arms; (ii) V-shaped TiO_2 rotors and SiO_2 spheres. Reproduced with permission from Ref. [51]. Copyright 2010, Wiley-VCH. (I) Schematic diagram showing the glancing angle deposition (GLAD) of a single-turn SiO_2/Pt helix and the SEM image of catalytic helical microdrills obtained through the multi-step GLAD processes. Reproduced from Ref. [52] with permission from The Royal Society of Chemistry. (J) (top) SEM images of (a) symmetric and (b and c) asymmetric rolled-up nanotubes; (middle) illustration of their motion; and (bottom) a micrograph showing the spiral trajectory of an asymmetrically rolled-up nanotube. Reprinted with permission from Ref. [53]. Copyright 2012 American Chemical Society. (K) Diffusiophoresis nanomotors propelled by the release of K^+ ions from the $(Pb_{0.25}Ba_{0.15}Sr_{0.6})TiO_3$ (PBST) nanotubes. Reprinted with permission from Ref. [54].

Copyright 2010, AIP Publishing LLC. (L) Schematic diagram of a ratchet-shaped Cu nanorod rotating in Br_2 solution. Reprinted with permission from Ref. [44]. Copyright 2011 American Chemical Society.

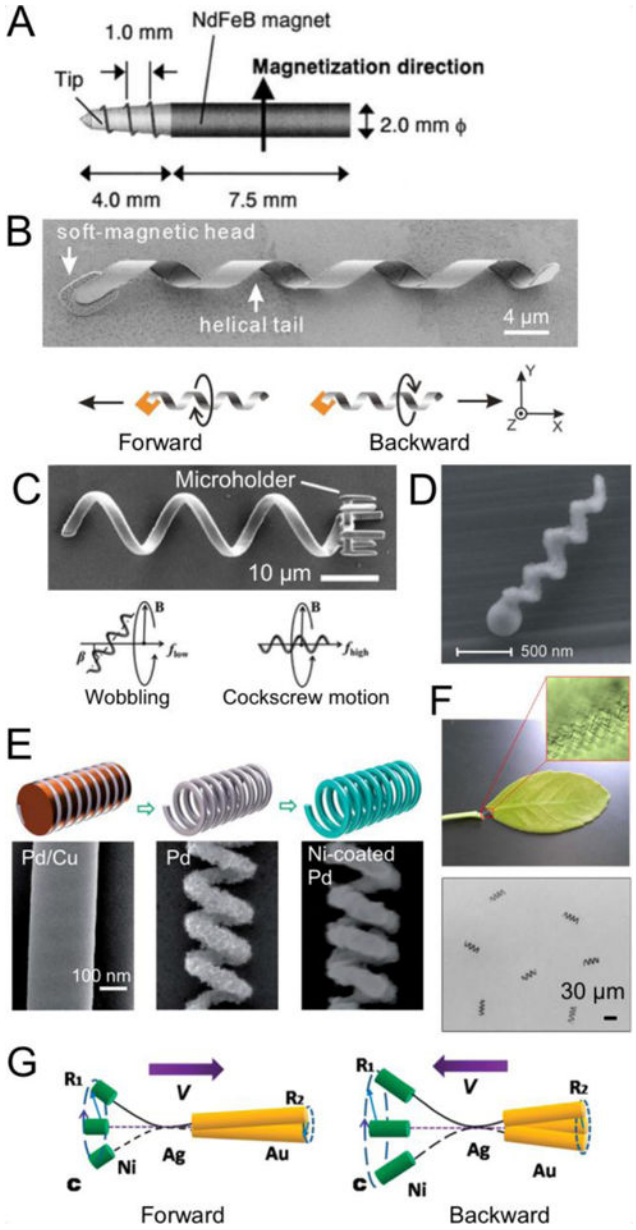

Figure 3. Magnetically driven helical micro/nanoswimmers

(A) NdFeB magnetic micromachine with a screw tip. Reprinted from Ref. [68], Copyright 2001, with permission from Elsevier. (B) SEM image of an artificial bacterial flagellum (ABF) with a Cr/Ni/Au magnetic head and a InGaAs/GaAs/Cr helix and the schematic diagrams showing its different motion modes. Reprinted with permission from Ref. [70]. Copyright 2009, AIP Publishing LLC. (C) SEM image of a microswimmer fabricated through 3-D direct laser writing (DLW) and the illustrations of its wobbling and cockscrew motion. Reproduced with permission from Ref. [73]. Copyright 2012, Wiley-VCH. (D) SEM image of a magnetic nanoswimmer fabricated through the GLAD of SiO_2 helix followed by Co deposition. Reprinted with permission from Ref. [17]. Copyright 2009 American Chemical Society. (E) Schematic diagrams and SEM images of a Pd/Cu nanorod, a Pd nanospring, and Ni-coated Pd nanospring obtained from template-assisted fabrication of magnetic helical

nanosprings. Reproduced from Ref. [82] with permission from The Royal Society of Chemistry. (F) Microswimmers based on the helical plant vessels. Reprinted with permission from Ref. [83]. Copyright 2014 American Chemical Society. (G) Illustration of the forward and backward motions of magnetic nanoswimmers comprised of Ni, flexible Ag, and Au segments. Reprinted with permission from Ref. [84]. Copyright 2010 American Chemical Society.

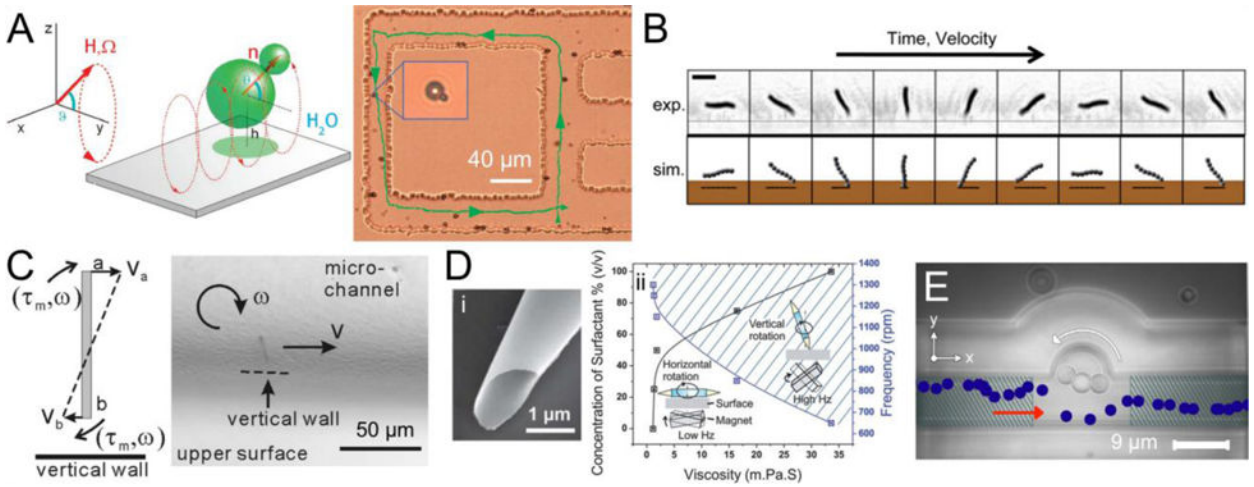

Figure 4. Magnetic nanomotors working near solid-liquid boundaries

(A) Rotating paramagnetic doublet moving along grooves patterned on the substrate. Reprinted with permission from Ref. [86]. Copyright 2008 American Chemical Society. (B) Experimental (exp.) and simulation (sim.) results of a self-assembled colloidal walker tumbling on the substrate. Reproduced from Ref. [88]. (C) Rotating Ni nanowire moving along a vertical wall due to the asymmetric boundary conditions at each end. Reprinted with permission from Ref. [89]. Copyright 2010 American Chemical Society. (D) (i) SEM image of a roll-up magnetic microdrill and (ii) the rotation mode of the microdrill, *i.e.*, the horizontal or vertical rotations, at different viscosity and angular frequency. Ref. [91] - Published by The Royal Society of Chemistry. (E) Microsphere assembly magnetically rotating counterclockwise in a microfluidic channel. The trajectory of a particle marked in blue shows the directional flow induced by the rotation. Reproduced with permission from Ref. [58]. Copyright 2014 IOP Publishing.

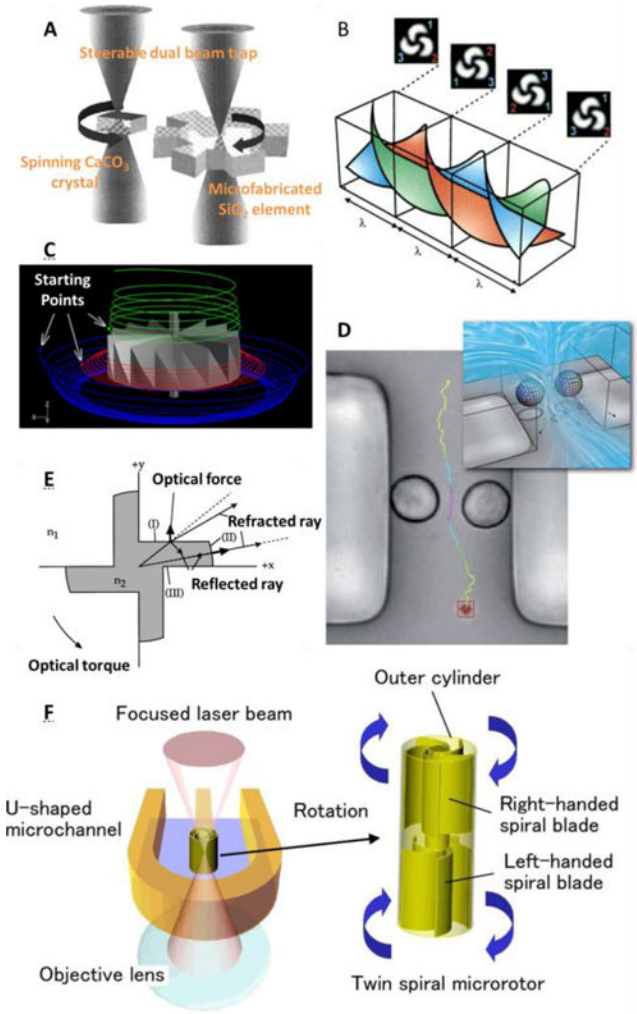

Figure 5. Optical nanomotors

(A) The spinning calcite crystal rotated by circularly polarized laser beam compelled the rotation of SiO_2 machines. Reprinted with permission from Ref. [100]. Copyright 2001, AIP Publishing LLC. (B) Phase fronts and intensity patterns of a helical mode laser beam of azimuthal index $l = 3$ obtained from its interference with a plane wave. From Ref. [104]. Reprinted with permission from AAAS. (C) A turbine-like micromotor and the resulted streamlines showing fluid circulation. Reprinted with permission from Ref. [108]. Copyright 2012, AIP Publishing LLC. (D) Two birefringent beads simultaneously trapped and rotated in opposite directions to drive flows in a 15-μm-wide PDMS channel. Reproduced from Ref. [109] with permission from The Royal Society of Chemistry. (E) Schematic showing the origin of the optical torque of radiation pressure micromotors. Reprinted with permission from Ref. [114]. Copyright 1997, AIP Publishing LLC. (F) Viscous micropumps based on twin spiral micromotors driven by radiation pressure. Reprinted with permission from Ref. [117]. Copyright 2009 Optical Society of America.

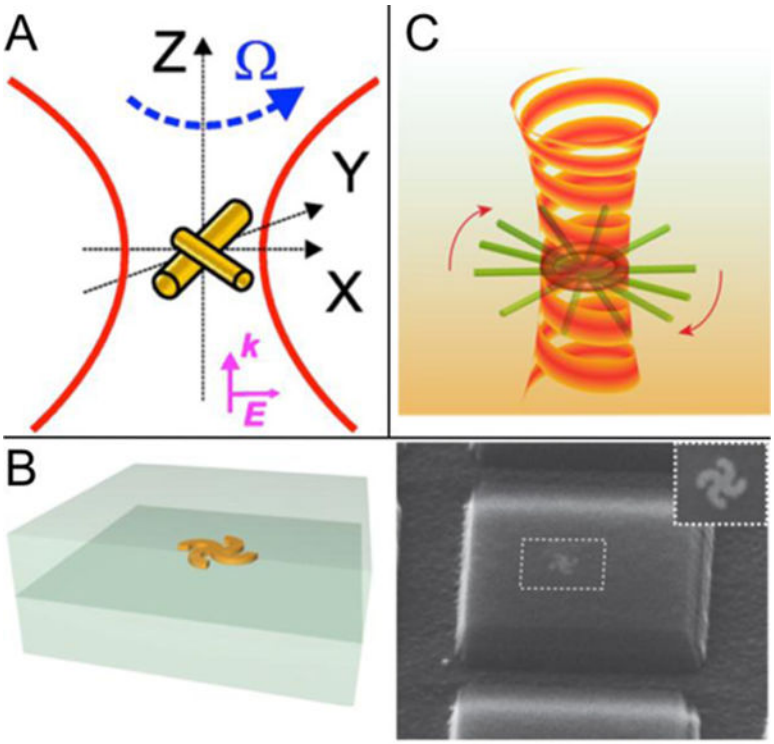

Figure 6. Plasmonic nanomotors

(A) Schematic diagram showing the rotation of a T-shaped Au nanorod assemblies. Reprinted with permission from Ref. [122]. Copyright 2009 American Chemical Society. (B) Illustration and SEM image of a nanoscale plasmonic motor. Reprint by permission from Macmillan Publishers Ltd: Nature Nanotechnology Ref. [16], copyright 2010. (C) Illustration of an optical vortex induced rotation of a single Ag nanowire on a glass surface. Reprinted with permission from Ref. [125]. Copyright 2013 American Chemical Society.

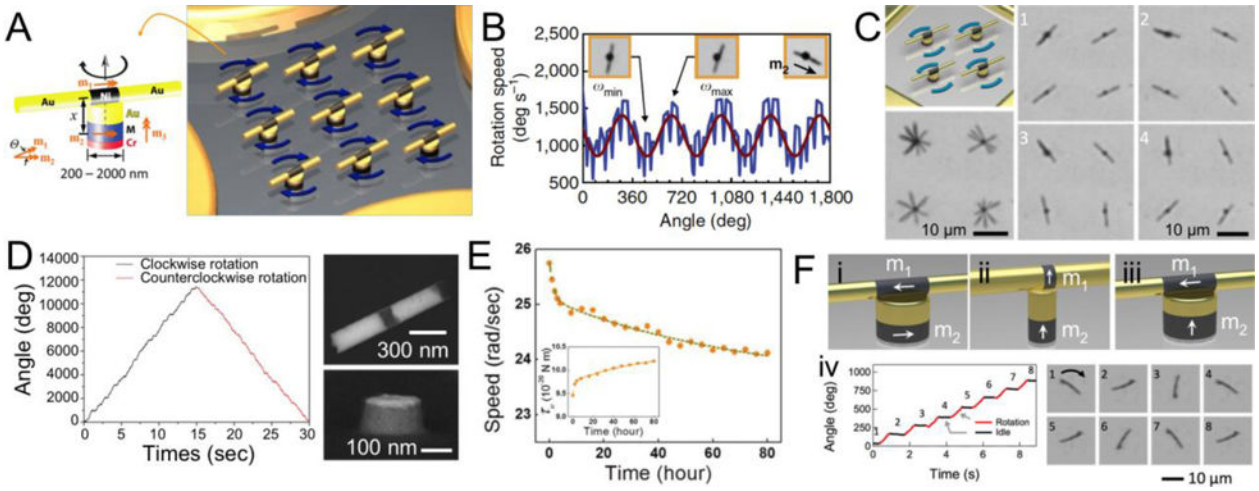

Figure 7. Electric field driven nanomotors

(A) Schematic diagrams of an ordered array of the nanomotors assembled from nanowires, patterned magnets and quadruple microelectrodes working as rotors, bearings, and stators. (B) Rotation speed of a nanomotor as a function of angle. (C) Illustration and sequential micrographs of a 2×2 array of nanomotors rotating simultaneously. (D) SEM images of a nanowire rotor and a patterned nanomagnet used for an ultrasmall nanomotor and its accumulative angle showing its controllability. Reproduced with permission from Ref. [15]. (E) Evolution of the rotation speed and the magnetic torque τ_M of a nanomotor during its 80-hour rotation. Reproduced from Ref. [55] with permission from The Royal Society of Chemistry. (F) Illustrations of the nanomotors with the (i) chopsticks; (ii) perpendicular; and (iii) T-shaped magnetic configurations depending on the relative magnetic orientations of the nanowires and the patterned magnets. (iv) Step-motor like angle control of the nanomotors with the T-shaped magnetic configuration. Reprinted with permission from Ref. [139]. Copyright 2015 American Chemical Society.

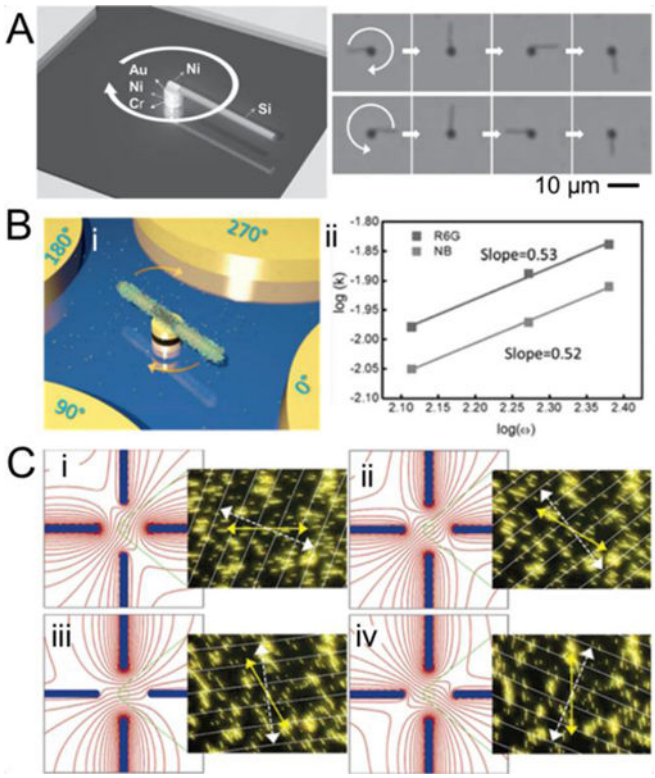

Figure 8.

(A) Clockwise and counterclockwise rotation of Si nanomotors assembled from Si/Ni nanowire rotors on Cr/Ni/Au magnets. Reproduced with permission from Ref. [137]. Copyright 2014, Wiley-VCH. (B) (i) Illustration of a nanomotor sensing and releasing biochemical molecules. (ii) Release rates (k) of Rhodamine-6G (R6G) and Nile Blue (NB) molecules increase with the rotation speed of the nanomotor ω (power law dependence of 0.53 and 0.52, respectively). Reproduced with permission from Ref. [142]. Copyright 2015, Wiley-VCH. (C) Sequential optical images of Au nanowires rotating synchronously. Images on the left: electric field simulations showing equipotential lines around the electrodes; Images on the right: the yellow solid and the white dashed lines indicate orientations of the nanowires and electric field, respectively. Reprinted with permission from Ref. [130]. Copyright 2006 American Chemical Society.

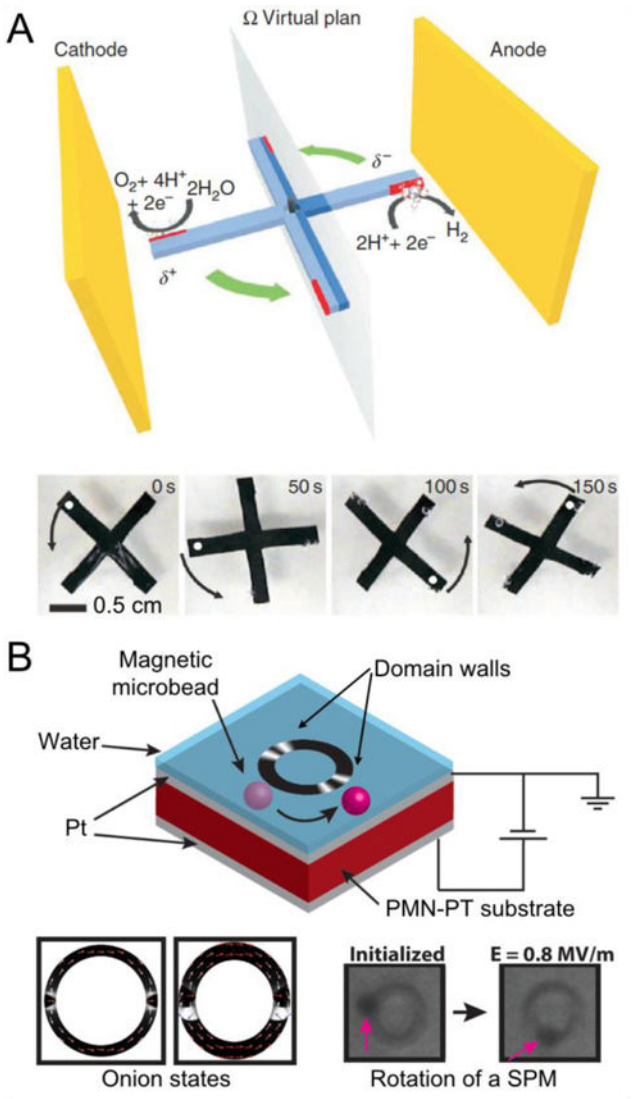

Figure 9.

(a) Schematic diagram of a bipolar electrochemistry powered rotor and rotation of a conducting polycarbonate sheet in 50 mM HCl and in an electric field of 0.5kV m^{-1}. The red areas are conducting and the blue areas are covered with an insulating polymer. Reprinted by permission from Macmillan Publishers Ltd: Nature Communications Ref. [148], copyright 2011. (B) Electric field controlled strain for rotation of the magnetic domain walls in Ni microrings, where the superparamagnetic microbeads (SPMs) attached on the microring rotate with the magnetic domain walls. Reprinted with permission from Ref. [149]. Copyright 2015 American Chemical Society.

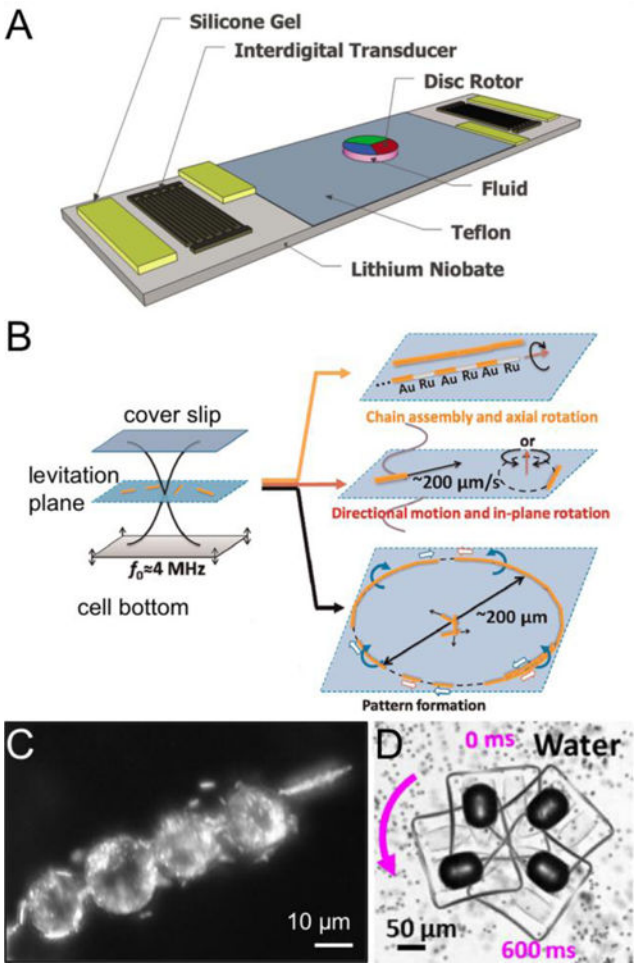

Figure 10. Acoustic nanomotors

(A) Schematic diagram of a SAW-driven micromotor. Reprinted with permission from Ref. [165]. Copyright 2011, AIP Publishing LLC. (B) Illustration of different types of linear and angular motion of AuRu nanorods on a levitation plain formed between the cover slip and the substrate in the presence of an acoustic field. Reprinted with permission from Ref. [154]. Copyright 2012 American Chemical Society. (C) Dark field image of a chain assembly of HeLa cells rotated by ultrasonic excitation with Au nanorods attached to their surface. Reproduced with permission from Ref. [159]. Copyright 2014, Wiley-VCH. (D) Overlaid image of sequential micrographs of acoustic-powered microswimmers rotating due to the oscillation of the asymmetrically trapped bubble. Reprinted with permission from Ref.[156].